Persistent KSHV infection increases EBV-associated tumor formation in vivo via enhanced EBV lytic gene expression.

Donal McHugh[1], Nicole Caduff[1], Mario Henrique M. Barros[2], Patrick Rämer[1], Ana Raykova[1], Anita Murer[1], Vanessa Landtwing[1], Isaak Quast[3,#], Christine Styles[4], Michael Spohn[5], Adeola Fowotade[6], Henri-Jacques Delecluse[7], Alexandra Papoudou-Bai[8], Yong-Moon Lee[9], Jin-Man Kim[9], Jaap Middeldorp[10], Thomas F. Schulz[11], Ethel Cesarman[12], Andrea Zbinden[13], Riccarda Capaul[13], Robert E. White[4], Martin Allday[4], Gerald Niedobitek[2], David Blackbourn[6±], Adam Grundhoff[5±] and Christian Münz[1*]

[1]Viral Immunobiology, Institute of Experimental Immunology, University of Zürich, Switzerland

[2]Institute of Pathology, Unfallkrankenhaus Berlin, Germany

[3]Neuroinflammation, Institute of Experimental Immunology, University of Zürich, Switzerland,

[4]Section of Virology, Faculty of Medicine, Imperial College London, UK

[5]Virus Genomics, Heinrich Pette Institute, Hamburg, Germany

[6]School of Biosciences and Medicine, University of Surrey, UK

[7]DKFZ unit F100/INSERM unit U1074, Heidelberg, Germany

[8]Department of Pathology, Faculty of Medicine, University of Ioannina, Ioannina 45110, Greece

[9]Departments of Pathology and Medical Science and, Chungnam National University School of Medicine, Daejeon, Korea

[10]Department of Pathology, VU University Medical Center and Cancer Center Amsterdam, The Netherlands

[11]Institute of Virology, Hannover Medical School, 30625 Hannover and German Centre of Infection Research (DZIF), Hannover-Braunschweig Site, Germany

[12]Department of Pathology and Laboratory Medicine, Weill Cornell Medical College, New York, USA

[13]Institute of Medical Virology, University of Zürich, Switzerland

[#]Currently: Department of Immunology & Pathology, Monash University, Melbourne, Australia

[±]Contributed equally

[*]To whom correspondence should be addressed: muenzc@immunology.uzh.ch

Short title: KSHV and EBV cooperation in tumor formation

SUMMARY

The human tumor viruses Epstein Barr virus (EBV) and Kaposi Sarcoma associated herpesvirus (KSHV) establish persistent infections in B cells and can cause primary effusion lymphoma (PEL) upon dual infection. So far, no in vivo model exists to study KSHV persistence and associated lymphomagenesis. Here, we report that EBV/KSHV dual infection of mice with reconstituted human immune system components enhanced KSHV persistence and tumorigenesis with plasma cell-like gene expression similar to PELs. KSHV persisted in EBV transformed B cells and was associated with early lytic EBV gene expression, resulting in increased tumor formation. Evidence of lytic EBV replication was also found in EBV/KSHV dually infected lymphoproliferative disorders of patients. Our data suggest that KSHV augments EBV-associated tumorigenesis via stimulation of lytic EBV replication.

Keywords

Epstein Barr virus, EBV, Kaposi Sarcoma associated herpesvirus, KSHV, primary effusion lymphoma, humanized mouse model, B cell lymphoma, virus-associated lymphoma

Significance

The first small animal model of Kaposi Sarcoma associated herpesvirus (KSHV) infection, which also exhibits a KSHV dependent pathology, demonstrates that this virus collaborates with another human gamma herpes virus, Epstein Barr virus (EBV), to establish persistent infection in B cells. Upon dual infection with both viruses EBV lytic gene expression is elevated and contributes to reduced survival and enhanced tumorigenesis in infected animals. The emerging transformed cells resemble in their gene expression primary effusion lymphomas (PEL), the tumors that are caused by EBV and KSHV dual infection in humans. Clinical PEL samples also display increased lytic EBV gene expression. Therefore, inhibition of lytic EBV replication could be therapeutically explored in PEL patients.

Highlights

- A novel mouse model for KSHV infection based on EBV/KSHV dual infection.
- KSHV relies on B cell transformation by EBV for more frequent persistent infection.
- KSHV promotes PEL and plasma cell-like gene expression in dual-infected cells.
- Enhanced tumorigenesis upon EBV/KSHV infection is driven by EBV lytic gene expression

INTRODUCTION

The human oncogenic viruses Epstein Barr virus (EBV) and Kaposi Sarcoma associated herpesvirus (KSHV) establish persistent infections in B cells (Ambroziak et al., 1995; Babcock et al., 1998). KSHV, originally discovered in Kaposi sarcoma (Chang et al., 1994), is associated with around 1% of all human tumors and classified as a WHO class I carcinogen (Bouvard et al., 2009; Parkin, 2006). Specifically, KSHV has been linked to the B cell lymphoproliferative disorders Multicentric Castleman's Disease (Soulier et al., 1995), which can progress to KSHV associated non Hodgkin lymphoma in up to 20% of cases (Oksenhendler et al., 2002), and primary effusion lymphoma (PEL) (Cesarman et al., 1995). Around 90% of PELs also contain EBV (Cesarman, 2014), which itself causes 1-2% of the total human cancer burden worldwide (Cohen et al., 2011). In contrast to EBV associated lymphomas like Burkitt (BL), classical Hodgkin and diffuse large B cell lymphomas (DLBCL), PELs resemble plasma cells with a transcriptional signature between multiple myeloma and EBV positive immunoblastic lymphoma (Jenner et al., 2003; Klein et al., 2003).

It is thought that gene expression of both viruses contributes to the proliferation and apoptosis resistance of PEL cells. Both viruses are capable of latent and virus-replicating lytic gene expression. The transforming capacities of EBV and KSHV are mediated by a number of latent proteins, which are not involved or differently regulated during infectious virus producing lytic infection. EBV expresses all eight of its latency-associated proteins during its transforming latency pattern. The nuclear antigens EBNA1, 2, 3A-C and LP, the two latent membrane proteins LMP1 and 2, as well as non-translated RNAs, the Epstein Barr virus encoded RNAs (EBERs) and viral miRNAs, are expressed during this transcription program, also termed latency III (Babcock et al., 2000). This latency III program is detected in naïve B cells of healthy EBV carriers (Babcock et al., 2000). In germinal center B cells only EBNA1, LMP1 and LMP2 are found. This latency II program is also detected in 40-50% of Hodgkin's lymphomas. Latency II is frequently termed IIa to distinguish it from ENBA2 expressing cells that lack expression of the LMPs (=IIb) (Klein et al.,

2013). Finally, EBNA1 is the only viral protein expressed in homeostatically proliferating memory B cells and EBV associated BL. This latency I program is further reduced for persistence without viral protein expression in non-replicating memory B cells. In this latency 0 program only non-translated viral RNAs are expressed (Babcock et al., 1998). In most PEL cell lines only EBNA1 protein expression is observed, and this latency I program in PEL seems to be complemented by growth transforming and apoptosis inhibiting gene products of KSHV (Cesarman, 2014). Of these, LANA fulfills similar functions to EBNA1 in maintaining episomal KSHV DNA in proliferating cells. In addition, it can inactivate the tumor suppressor p53 (Friborg et al., 1999) and stabilize the oncogene product c-myc (Bubman et al., 2007). Furthermore, the KSHV K15 and K1 gene products fulfill some of the anti-apoptotic functions of EBV's LMP2 (Brinkmann et al., 2003; Sharp et al., 2002; Steinbruck et al., 2015). From the same transcript that encodes LANA two additional latent KSHV proteins are translated. The viral FLICE/caspase 8 inhibitory protein (vFLIP) activates NF-κB, which in turn up-regulates anti-apoptotic proteins (Guasparri et al., 2006). The other co-transcribed gene product, viral cyclin, interacts with CDK6 to drive the cell cycle of infected cells (Godden-Kent et al., 1997; Li et al., 1997). In addition, viral IL-6, encoded by K2, promotes B cell survival (Moore et al., 1996). Interestingly, KSHV lytic gene expression has also been implicated in Kaposi Sarcoma (Martin et al., 1999) and increasingly there is evidence that EBV lytic gene expression also plays a role in lymphomagenesis (Antsiferova et al., 2014; Chijioke et al., 2013; Hong et al., 2005; Ma et al., 2011; Ma et al., 2012).

So far, most investigations of KSHV associated PEL biology have been performed in vitro with PEL cell lines or via the direct examination of primary patient material. Studies on persistent KSHV infection in vivo, its pathogenicity and the role of EBV co-infection in PEL development have been hampered by the absence of a small animal model that enables KSHV persistence without repeated inoculation (Wang et al., 2014) and that replicates KSHV associated tumorigenesis. In this study we investigated if EBV co-infection could support KSHV persistence and tumorigenicity in a novel humanized mouse model of dual infection with these human oncogenic γ-herpesviruses.

RESULTS

KSHV persists more frequently in the presence of EBV in huNSG mice and enhances tumor formation. Based on our earlier observations that dual infection of umbilical cord blood mononuclear cells with EBV and KSHV enabled KSHV persistence in vitro (Blackbourn et al., 2000) and in keeping with the ubiquity of EBV infection in humans (Taylor et al., 2015), NOD-*scid* $\gamma_c^{-/-}$ mice with human immune system components reconstituted from $CD34^+$ hematopoietic progenitor cells (huNSG) were infected with recombinant KSHV (rKSHV.219, based on the JSC1 KSHV strain and encoding GFP under the huEF-1α promoter; (Vieira and O'Hearn, 2004)) and/or recombinant EBV (p2089, based on the B95-8 EBV strain and encoding GFP under the IE-CMV promoter; (Feederle et al., 2000)). Survival of the EBV+KSHV dually infected animals was significantly reduced compared to EBV single infected mice (Fig.1A), which in our previous studies would survive up to 6 weeks post infection (Antsiferova et al., 2014; Chijioke et al., 2013). Furthermore, the EBV and KSHV dually infected animals exhibited significantly more frequent tumor presence in the spleen or peritoneal cavity (Fig.1B) and a higher EBV burden in the spleen (Fig.1C), whereas KSHV single infection did not lead to any macroscopically visible pathology. KSHV persistence, evaluated by detection of KSHV DNA via qPCR in the spleen and blood, was more frequent in dually infected huNSG mice compared to KSHV single infected huNSG mice (Fig.1D) and seemed to correlate with enhanced tumor formation (Fig. S1B). Immunohistochemistry for KSHV's Latent Nuclear Antigen (LANA) in the spleen up to 4 weeks post infection confirmed more frequent persistence of KSHV upon EBV co-infection (Fig.1E&F). Both LANA and EBNA2 expression were detected mostly within B cells (Fig.1E&G). Moreover, co-infection of cells with EBV and KSHV in vivo could be demonstrated by LANA and EBV latent membrane protein 1 (LMP1) co-staining albeit at a slightly lower frequency compared to EBNA2 co-expression with LMP1 in cells of EBV or EBV+KSHV dual-infected animals (Fig.1H&I). We used GFP expression as a surrogate marker for KSHV infection in dual-infected cells, since GFP-

expression resulting from recombinant EBV in huNSG mice can hardly be detected, likely due to rapid methylation of the EBV genome in vivo upon infection ((Woellmer et al., 2012) and Fig.S1C-E). In peritoneal lavage and splenic samples from dually infected animals we found that GFP$^+$ cells expressed huCD45 and were partially positive for CD19 but for no other lymphocyte lineage markers, confirming that KSHV infects mostly human B cells in this model (Fig.1J and not shown). Using an RNA in situ hybridization method adapted to flow cytometry, we could further show that the majority of the KSHV infected (GFP$^+$) splenocytes also harbored the highly abundant EBV EBER1-2 transcripts (Fig.1K), indicating that EBV transformed cells were among the primary KSHV targets and likely facilitated its persistence in this model. In summary, KSHV persists in the majority of huNSG mice upon infection with EBV and dual infection leads to a higher EBV burden, increased tumor formation and reduced survival. Furthermore, both viruses can frequently be found in the same cells, consistent with previously reported KSHV infection of EBV transformed B cells in vitro (Kliche et al., 1998).

Tumor cell lines derived from EBV and KSHV dual-infected animals harbor both viruses and exhibit KSHV expression. In order to characterize the dually infected tumors in more detail, cells from spleen, tumors or peritoneal lavage of virus-infected huNSG mice were cultured in vitro until cell lines could be expanded. These sources never yielded cell lines from KSHV single-infected animals. In contrast, cell lines could be derived from EBV and EBV+KSHV dually infected animals and their cellular EBV genome content was similar (Fig.2A). Dually infected cell lines enriched for cells with higher GFP encoding KSHV genome copy numbers (Fig.S1C-E) reached KSHV DNA contents as high as, but mostly lower than human PEL derived cell lines (Fig.2A). Depletion of GFP expressing cells led to a complete loss of KSHV transcription from the established cell lines, indicating that only the subset of GFP expressing cells was infected with KSHV (Fig.S1F). Indeed, co-immunohistochemistry for EBV LMP1 and KSHV LANA suggested that individual cells in lines derived from EBV+KSHV dually infected huNSG mice were a mixture of KSHV$^+$ and KSHV$^-$ cells, with many of the former co-expressing antigens from both viruses

(Fig.2B). Furthermore, all cell lines were of B cell origin based on their surface expression of CD19 (Fig.S1G). RNA sequencing of selected cell lines derived from dually infected huNSG mice confirmed active KSHV transcription that was generally comparable to human PEL derived cell lines (Fig.2C, Datasets S1&2). Based on their KSHV transcription these cells did not cluster entirely separately from five established PEL cell lines or with the 3 EBV$^+$/KSHV$^+$ PEL cell lines (Fig.2D). Thus, KHSV gene transcription in the EBV and KSHV dually infected cell lines is similar to human PEL cell lines.

EBV and KSHV dual-positive tumor cell lines show hallmarks of PEL and plasma cell differentiation. Analysis of the host transcriptome revealed a distinct cellular transcription pattern in EBV$^+$/KSHV$^+$ cell lines compared to those derived from EBV-single infected mice (Fig.3A, Dataset S3) as seen by the clustering of the EBV$^+$ and EBV$^+$/KSHV$^+$ cell lines respectively in a principal component analysis (Fig.3B). Dually infected cell lines showed an increased abundance of genes associated with mitochondrial function, mitotic cell cycle, negative regulation of apoptotic processes, as seen using gene ontology (GO) and Kyoto Encyclopedia of Genes and Genomes (KEGG) pathway analysis. Conversely, genes involved in innate immune responses and cytokine signaling were down-regulated (Fig.3C, Dataset S4). Thus, KSHV presence could lead to reduced cell death, dampened innate immune responses and enhanced proliferation. Hierarchical clustering based on the differentially regulated cellular genes between EBV$^+$ and EBV$^+$/KSHV$^+$ cell lines showed clustering of the 2 EBV$^+$ huNSG derived cell lines with 3 in vitro EBV transformed lymphoblastoid cell lines (LCLs) and the 3 EBV$^+$/KSHV$^+$ cell lines with 5 PEL cell lines (Fig.3D & Datasets S5&6, full heat map and gene cluster in Fig.S2A). Furthermore, in gene set enrichment analysis (GSEA) the EBV$^+$/KSHV$^+$ cell lines demonstrated a more PEL and plasma cell-like gene expression pattern compared to EBV single infected huNSG derived cell lines, including a higher abundance of genes typically expressed in PELs (Jenner et al., 2003; Klein et al., 2003), such as Aquaporin 3 (*AQP3*), BLIMP1 (*PRDM1*) and IRF4 (also termed MUM1, *IRF4*) (Fig.3E; Fig.S2B and Datasets S7&8). IRF4 and BLIMP1 protein were confirmed to be up-

regulated, whereas CD40 and CD19 surface expression was down-regulated (Fig. 3F&G). In line with these in vitro findings a trend toward more IRF4^{high} B cells was found in spleens of dual-infected huNSG. Moreover, the putatively KSHV infected (GFP$^+$) cells in these mice expressed high levels of IRF4 more frequently than the overall B cell populations in any of the infected animals. (Fig.S2C). Overall the histological phenotype of the virally induced lymphoproliferations in the spleen of either EBV or EBV+KSHV infected huNSG was CD20$^+$, CD10$^–$, BCL6$^–$, MUM1$^+$ indicating a non germinal center (non-GC) phenotype with a small trend towards more CD138$^+$ cells in the dual infected animals (Fig.1E, Fig.S2D&E), in line with the MUM1$^+$BCL6$^–$CD138$^+$ phenotype frequently found in human PEL cases (Carbone et al., 2001). Taken together, the presence of KSHV in cell lines expanded in vitro from EBV+KSHV dually infected huNSG mice seems to be associated with a shift in host gene expression towards a more PEL- and plasma cell-like phenotype.

EBV and KSHV dual-positive tumor cell lines show enhanced EBV lytic gene expression. Since plasma cell differentiation and BLIMP1 expression specifically have been associated with EBV lytic reactivation (Laichalk and Thorley-Lawson, 2005) and this could explain the elevated tumor formation in vivo, we investigated EBV gene expression in EBV$^+$/KSHV$^+$ cell lines derived from infected huNSG mice. All dually infected lines expressed the full range of EBV latent genes indicating a type III latency pattern (Dataset S9), yet there was evidence of increased transcription through the locus of the immediate early transactivator of EBV lytic replication, BZLF1, along with other early lytic genes (Fig.4A and supplementary dataset S9), concomitant with an overall reduction of viral reads by approximately 50% (Dataset S1). Confirming these results, a higher expression of *BZLF1,* a lower expression of the latency III *Cp/Wp*-promoter driven EBNA1 transcript and a trend toward lower expression of EBNA2 was found by RT-qPCR in the EBV$^+$/KSHV$^+$ cells. *LMP1* and *LMP2A*, however, did not seem to be differentially regulated in EBV$^+$/KSHV$^+$ cell lines indicating only a partial recapitulation of the transcription pattern of chemical lytic induction of EBV$^+$ cell lines with phorbol-12-myristate-13-acetate and sodium

butyrate (TPA/NaB) (Fig.4B). In line with an early EBV lytic activity, EBV$^+$/KSHV$^+$ cell lines also contained a higher frequency of cells expressing BZLF1 protein (Fig.4C). Moreover, we observed a trend toward lower EBNA2 and EBNA3B protein expression coupled with higher overall levels of early lytic cycle proteins BZLF1 and BALF2 in EBV$^+$/KSHV$^+$ cells. Late lytic EBV antigens were not detected, indicating primarily an early (abortive) lytic cycle in EBV$^+$/KSHV$^+$ cell lines (Fig. 4D). Finally, BZLF1$^+$ cells were found more often in splenic sections from dually infected animals (Fig.4E and Fig.S3A). EBV infected huNSG mostly harbor EBV infected cells expressing the latency III (or IIb) antigen EBNA2 (Fig.1). Interestingly, in dual-infected animals we could see a small percentage of cells, which lacked EBNA2 but retained EBNA1 (=latency I) or EBNA1 and LMP1 expression (=latency II) (Fig.4F & S3B). Collectively, it seems that the PEL and plasma cell like expression pattern in dually infected cell lines is also associated with increased EBV lytic and reduced EBV latency III gene transcription.

EBV lytic gene expression leads to enhanced tumorigenesis in EBV and KSHV dual-infected mice. In order to investigate whether KSHV induced EBV lytic activity also mediated enhanced tumorigenesis and elevated EBV burden, we tested KSHV co-infection with a recombinant EBV mutant that is no longer able to activate lytic replication due to loss of BZLF1 (EBVzko) (Feederle et al., 2000). Upon EBVzko+KSHV co-infection overall survival was high and similar to EBVzko single-infected animals (Fig.5A). Furthermore, macroscopic tumor formation was significantly less frequent in EBVzko+KSHV infected animals compared to EBVwt+KSHV infected huNSG mice (Fig.5B). Additionally, the higher splenic EBV burden observed during EBVwt+KSHV dual infection compared to EBVwt single-infection was not observed upon dual infection with EBVzko (Fig.5C). Therefore, the presence of BZLF1 seems necessary for the pathology observed during dual infection with EBV and KSHV. LANA expression, however, was detected as frequently in splenic histological sections of mice dually infected with either EBVwt+KSHV or EBVzko+KSHV (Fig.5D). In line with these data, KSHV DNA was detected at similar if not lightly higher levels (Fig.5E) and as frequently in the blood or spleen of EBVwt+KSHV

or EBVzko+KSHV dually infected huNSG mice (Fig.5F), further arguing that the ability to readily switch into EBV lytic replication is dispensable for enhanced KSHV persistence. Moreover, when transplanted into non-reconstituted NSG mice, $EBV^+/KSHV^+$ cells derived from huNSG mice seemed to generate tumors at a similar or even lower rate compared to EBV^+ cells (Fig. 5G). This further indicates that these dual-infected cells do not have a growth advantage per se, but rather that enhanced tumorigenesis during dual infection is mainly due to lytic EBV replication and is dependent on a surrounding lymphoid compartment. In line with such a lymphoma nurturing microenvironment, we found a trend toward higher serum cytokine levels in huNSG mice infected with EBVwt compared to EBVzko with and without KSHV co-infection (Fig. S4). Taken together, these data reveal that enhanced EBV lytic activity is associated with KSHV persistence in dually infected cells and seems to be responsible for the increased tumorigenesis observed in dually infected huNSG mice.

EBV lytic gene expression is elevated in patient-derived EBV and KSHV dual-infected lymphoproliferations. In order to investigate whether EBV lytic reactivation occurs in dually infected B cells of patients more frequently, we examined patients' $EBV^+/KSHV^+$ lymphomas including PELs and unconventional dually infected lymphoproliferations such as 2 cases described in detail in (Papoudou-Bai et al., 2015) and one case of plasmablastic microlymphoma arising in Multicentric Castleman's disease described in detail in (Lee et al., 2017) ($EBV^+/KSHV^+$ BCL). This analysis revealed evidence of EBV lytic activity via staining for EBV BZLF1 and viral capsid antigen (VCA) (Fig.6A). In contrast, when we analyzed lymphomas that exhibited low to no expression of plasma cell markers (e.g. BLIMP1, data not shown) like EBV^+ non-GC type DLBCL or $BLIMP1^-$ EBV^+ BL (EBV^+ BCL), $BZLF1^+$ and VCA^+ cells were rare or absent (Fig.6B). We enumerated the frequency of both $BZLF1^+$ and VCA^+ tumor cells from patients with and without HIV co-infection. $EBV^+/KSHV^+$ BCL had a higher number of cells with EBV lytic activity compared to EBV^+ lymphomas (Fig.6C&D). Furthermore, in the subset of patients, which did not have HIV infection as co-morbidity, this difference seemed to be even more pronounced

(red bars in Fig.6C&D). Lastly, a case of GC DLBCL, which was strongly positive for BLIMP1, also exhibited BZLF1 expression (Fig.6E), demonstrating that the EBV lytic reactivation is associated with plasma cell like differentiation, which in the case of dually infected lymphoproliferations seems to be associated with KSHV presence.

DISCUSSION

Our studies have resulted in a small animal model for KSHV infection and associated B cell lymphoproliferation. Importantly, our data reveal that KSHV can persist more frequently in vivo during dual infection with EBV and that both herpes viruses reside within the same transformed cells. EBV's immediate early lytic transactivator BZLF1 was dispensable for KSHV persistence during dual infection, indicating that EBV's B cell transforming capabilities are sufficient for facilitating KSHV infection in vivo. These dually infected B cells may represent a model of $EBV^+/KSHV^+$ lymphoma precursors since they exhibit a host gene expression akin to PEL, but unlike PEL are not clonal. It is conceivable that with the acquisition of additional cellular mutations individual cells from the dually infected bulk populations could become increasingly independent of the transforming EBV latent gene expression pattern (latency III) and develop into clonal lymphomas. In line with our findings is the fact that around 90% of PEL cases exhibit dual infection of lymphoma cells with EBV (Cesarman, 2014) and that the remaining 10% may rely more on the deregulation of the mitogen-activated protein kinase pathway to compensate for the lack of EBV-driven transformation (Fan et al., 2005). Indeed, of the two γ-herpesviruses, EBV seems to be the superior transforming virus since it can readily transform B cells into indefinitely growing lymphoblastoid cell lines upon infection in vitro, whereas KSHV cannot.

Interestingly, in our model, increased EBV lytic gene expression and associated tumorigenesis is achieved upon co-infection with KSHV. The concept that lytic viral replication supports tumorigenesis may seem counterintuitive at first. However, in the case of EBV infection, which can transform human B cells in vitro in the absence of lytic transactivators (Feederle et al.,

2000), lytic replication has been suggested to contribute to lymphoma development in vivo (Antsiferova et al., 2014; Chijioke et al., 2013; Hong et al., 2005; Ma et al., 2011; Ma et al., 2012). In these studies very limited late EBV protein expression was detected during EBV infection, and therefore did not correlate with the observed tumor formation. This observation suggests that viral DNA replication itself might not induce the pro-lymphomagenic effects of lytic EBV replication, but instead that early lytic antigens contribute to the production of paracrine growth factors for tumor cells. Indeed, early EBV lytic transcripts and antigens such as BZLF1 have been previously reported in dually infected PELs and PEL cell lines (Cannon et al., 2000; Horenstein et al., 1997). In line with this, EBV copy numbers in circulating cell-free (CCF) DNA, which is a surrogate marker for lytic EBV replication has been found to correlate well with EBV associated malignancy burden, risk to develop EBV positive lymphomas in immune suppressed conditions and EBV associated tumor relapse after treatment (Kanakry and Ambinder, 2015). For example, rising EBV copy numbers in CCF DNA of bone marrow transplant patients predict the development of post-transplant lymphoproliferative disease (PTLD) and can be used as an indication to start B cell depleting therapy to decrease the risk for lymphoma formation (van Esser et al., 2002; van Esser et al., 2001). Moreover, the viral Bcl-2 homologues BALF1 and BHRF1, considered to be early lytic EBV antigens, were found to be expressed early during B cell transformation to ensure the survival of newly infected B cells before EBNA2 driven proliferation ensues (Altmann and Hammerschmidt, 2005). In addition, different viral strains vary in their ability to activate the lytic infection cycle spontaneously (Tsai et al., 2017). While infection with some of these EBV strains would lead to less efficient transformation of purified human B cells, others retain efficient B cell transformation despite elevated lytic replication. The latter EBV strains might counterbalance their destruction of infected B cells by lytic replication with the pro-oncogenic contributions of lytic EBV infection. Thus, EBV lytic replication might contribute to lymphomagenesis by elevated B cell transformation or even by conditioning of the tumor microenvironment for more efficient lymphoma growth. KSHV does not readily transform cells in vitro and its latent infection program (LANA, v-

cyclin, v-FLIP, Kaposins A, B and C as well as viral miRNAs) might mainly ensure persistence and replication of the viral DNA in dividing host cells (Ganem, 2006) as well as shape the distinct cellular gene expression profile found in PEL (Fan et al., 2005). Sin and Dittmer found, that when the KSHV latent transcript LANA, v-cyclin, v-FLIP including the viral miRNAs were expressed transgenically in C57BL/6 mice, this led to enhanced plasma cell formation (Sin and Dittmer, 2013; Sin et al., 2015). Arguing for a contribution of lytic KSHV infection to tumorigenesis, a significantly lower incidence of Kaposi sarcoma was found in AIDS patients that had been previously treated with herpes virus DNA polymerase inhibitors during human cytomegalovirus reactivation (Martin et al., 1999). Thus, both EBV and KSHV lytic gene expression might contribute to tumorigenesis by these γ-herpesviruses and prevention of lytic replication could be a promising approach to counteract tumor formation induced by the collaboration of these two oncogenic viruses.

EXPERIMENTAL PROCEDURES

Humanized mouse generation and infection with EBV and KSHV

NOD/LtSz-scid IL2Rgnull (NSG) mice were obtained from the Jackson Laboratory and bred and maintained at the Institute of Experimental Immunology, University of Zurich, under specific pathogen-free conditions. Newborn NSG mice (1 to 5 days old) were irradiated with 1 Gy. Five to seven hours after irradiation, mice were injected intrahepatically with 1–3x10^5 $CD34^+$ human hematopoietic progenitor cells derived from human fetal liver tissue obtained from Advanced Bioscience Resources. Isolation of human $CD34^+$ cells from human fetal liver tissue was performed as described previously (Strowig et al., 2009; White et al., 2012). Individual mouse cohorts were reconstituted with cells derived from eight different donors. Reconstitution of human immune system components in mice was analyzed 10-12 weeks after engraftment and again before the start of the experiments by flow cytometric immune phenotyping of PBMCs (as previously described (Antsiferova et al., 2014)). Average $huCD45^+$ cells of peripheral blood

lymphocytes before experiment was 79.3% ± 11.8%, huCD3$^+$ T cells of huCD45$^+$ 33.5% ± 14.7%, huCD19$^+$ B cells of huCD45$^+$ 58.0% ± 14.0%, huCD4$^+$ T cells of human T cells 71.7% ± 9.3%, huCD8$^+$ T cells of human T cells 25.5% ± 9.1%, CD3$^-$ NKp46$^+$ NK cells of human lymphocytes 2.3% ± 1.2%, (Mean ± SD, n=119). Eleven to twenty-three weeks after engraftment, huNSG mice were injected with 10^5 RIU of EBVwt or EBVzko, 10^{5-7} IU of KSHV, injected with both EBV and KSHV or PBS intraperitoneally. Each experiment was performed with a cohort of mice reconstituted with CD34$^+$ cells from a single donor. Animals were sacrificed four weeks post infection or between three to four weeks post infection if necessitated by the laboratories animal welfare protocol due to general health symptoms and weight loss over 15%. EBV inoculated mice with no EBV DNA load in blood and spleen and no EBV nuclear antigen staining or EBER in situ hybridization in FFPE splenic sections at 4 weeks post infection were considered non-infected and were excluded from analysis. The tumor frequency in mock, KSHV, EBV and EBV/KSHV dually infected huNSG mice was assessed by a tumor score: no tumors observed = 0; tumor observed = 1; multiple tumors observed = 2. Animal protocols were approved by the veterinary office of the canton of Zurich, Switzerland (protocol nos. 116/2008, 148/2011 and 209/2014).

Generation of cell lines derived from infected huNSG mice

Single cell suspensions were prepared from mechanically disrupted spleens, tumors or terminal peritoneal lavage (terminal peritoneal lavage performed as previously described by (Ray and Dittel, 2010)) and cultured in RPMI 1640 medium supplemented with 8% FBS, 50U/ml penicillin-streptomycin and 1% glutamine (R8) with or without co-culture of irradiated CD40L expressing fibroblasts. Within cultures of KSHV and EBV positive cell lines, the expression of GFP, encoded by both recombinant viruses, was found to correlate with KSHV but not EBV genome content. After at least 1 month of culture selected cell lines were sorted for GFP expression by flow cytometry with an Aria III 5L sorter (BD Biosciences) in order to increase the mean KSHV content

per cell. GFP^+ and in some cases GFP^- fractions were cultured as suspension cell lines and expanded, GFP sorting was repeated up to 3 times for selected cell lines.

Generation of luciferase expressing cell lines and transplantation into NSG

An EBV^+ and an $EBV^+/KSHV^+$ cell line (E4-9s and EK3-13, respectively) were cultured for one day in lentivirus containing culture supernatants, diluted 1:1 with R8. Thereafter, cells were washed extensively and cultured in R8 for three days. Transduced cells were selected by culture in the presence of 5µg/ml blasticidin for one month and luciferase activity was confirmed in vitro. Transduced cells were washed and resuspended in PBS, 10^7 cells were injected intraperitoneally into 5-6 month old non-reconstituted NSG mice in a volume of 200µl. In vivo bioluminescent imaging was performed once weekly for 4 weeks with Xenogen IVIS100 Imaging System (Caliper Life Sciences) upon application of 100mg/kg bodyweight of D-Luciferin (Perkin Elmer) as previously described (Vom Berg et al., 2013). Data were subsequently analyzed using Living Image software (Caliper Life Sciences). A rectangular region of interest (ROI) was set to include the entire abdomen and thorax region of each mouse and photon flux within the ROI was read out. The generation of the luciferase encoding lentivirus can be found in the supplemental material.

Immunohistological analysis of mouse and patient sections

For the detection of latent EBV infection sections obtained from formalin-fixed, paraffin-embedded (FFPE) tissue samples were subjected to in situ hybridization (ISH) for EBV-encoded RNAs (EBER-ISH) as described previously (Meyer et al., 2011), employing diaminobenzidine (DAB) as chromogen (Zytomed Systems, Berlin, Germany). Immunohistochemical reactions for the detection of BZLF1 immediate early protein (clone BZ1, Santa Cruz), EBV p40 protein of the VCA complex (clone OT41, provided by J. Middeldorp, Amsterdam, The Netherlands), CD138 (clone SP152, Zytomed Systems), MUM1 (clone MUM1p, Dako), CD10 (clone 56C6, Zytomed Systems), BCL6 (clone GI191E/A8, Zytomed Systems) or LANA (clone LN35, Abcam) were carried out on a

Bond-III slide stainer (Leica Microsystems, Wetzlar, Germany) using diaminobenzidine (DAB) as chromogen. Double labeling immunohistochemistry was performed as described previously (Barros et al., 2013). Briefly, antigen retrieval was performed by heat treatment in a pressure-cooker for 1 minute with HIER-EDTA Buffer (Zytomed Systems, Berlin, Germany). After incubation with appropriately diluted EBNA2 (clone PE2, kind gift from M. Rowe, Birmingham, UK) or LANA (clone LN35, Abcam) primary antibodies (30 minutes), immobilized antibodies were detected using ZytoChem Plus HRP polymer kit (Zytomed Systems, Berlin, Germany), employing DAB as substrate. Subsequently, slides were washed in Wash Buffer (Zytomed Systems, Berlin, Germany) for 5 minutes and the appropriately diluted LMP1 (clones CS1-4, Zytomed Systems) or CD20 (clone L26, Dako) antibodies were applied overnight at 4^{o}C. Following another washing step using Wash Buffer (Zytomed Systems, Berlin, Germany), bound antibodies were detected using the AP Polymer System (Zytomed Systems, Berlin, Germany), employing Blue Alkaline Phosphatase (Vector Laboratories, California, USA) as substrate. The sections were not counterstained. The procedure for Triple labeling immunohistochemistry can be found in the supplemental experimental procedures. The quantification of labeled cells was performed using the image analysis software HISTO (Biomas) as described previously (Barros et al., 2012). For the estimation of the relative amount of BZLF1 or CD138 expressing cells per spleen in individual huNSG mice the quantification of positive cells/mm^2 in the biopsy was scaled up based on the total spleen weight for each mouse. For double labeling immunohistochemistry of cell lines with LMP1 and LANA on a BOND-MAX automated immunohistochemistry system (Leica Microsystems) sections of 4µm from FFPE blocks of centrifuged cells were deparaffinized, then antigen retrieval was performed by incubation in Bond^{TM} Epitope Retrieval Solution 2 (ER2, Leica) for 20min at 95°C followed by incubation with a mixture of mouse anti-LMP1 (Clones CS1, CS2, CS3 and CS4; NCL-EBV-CS1-4, Leica) antibodies, which were detected with the Refine HRP-Kit and DAB (Leica). Sections were then incubated in ER2 for 30min at 100°C before incubation with a mouse anti-LANA (Clone 13B10, Cell Marque Lifescreen Ltd.) antibody, which was detected

with the Refine AP-Kit and new fast red (Leica). Control stainings using the Refine HRP- and AP-Kits without prior incubation with the primary antibody mixtures for LMP1 or LNA were also performed. Nuclei were counterstained with haematoxylin (AP refine Kit, Leica). All images were white set point adjusted with Adobe Ps CS5 V12.1.

Statistical analysis

Unless otherwise stated, data with a Gaussian distribution were compared with a two-tailed unpaired t test or a two-tailed unpaired t test with Welch's correction if variances were significantly different as determined by the F test. Matched samples were compared with a two-tailed paired t test. Data with a non-Gaussian distribution were compared with a two-tailed Mann-Whitney test (MWT). The D'Agostino & Pearson omnibus test was used to test the normal distribution of data. Survival curves were compared with a log-rank test. Contingencies between categorical data were assessed with a two-tailed Fischer's exact test. A p-value of < 0.05 was considered statistically significant.

High-throughput sequencing and RNA-seq analysis

RNA was extracted from cell lines upon lysis in RNA Bee (Amsbio) according to the recommendations of the manufacturer. Strand-specific RNA-seq libraries were generated using the NEXTflex Directional RNA-Seq Kit (Bioo Scientific) according to the manufacturer's instructions. Libraries were sequenced on an Illumina HiSeq 2500 platform (paired end, 2x100 cycles) at an average depth of ~100 million reads per sample (see Dataset S1 for sequencing depth in individual samples). Three independent biological replicates from each human donor- or huNSG-derived cell lines were sequenced. One replicate from the huNSG-derived line EK 3-13 had to be excluded from further analysis due to high frequency of PCR duplicates. The five different PEL lines were sequenced as singletons. Transcription patterns across the genomes of EBV and KSHV were evaluated by mapping the first read of each RNA-seq read pair to the RefSeq

sequences NC_007605 and NC_009333, respectively, using the large gap read mapping tool of CLC Genomics Workbench v9.0 (Qiagen). The complete read coverage data is provided in Datasets S2 and S3, respectively. For analysis of gene expression, paired-end reads were mapped to annotated transcripts from the human genome assembly hg19 and the viral RefSeq entries with the RNA-seq analysis tool of the Genomics Workbench. As the individual samples differ in their EBV and KSHV infection status, principal component analysis was restricted to reads originating from host transcripts. Statistical analysis of differential host gene expression in EBV^+ and $EBV^+/KSHV^+$ huNSG-derived cell lines was performed with the proportion-based analysis tool of the CLC Genomics Workbench. Genes with a mean absolute fold change of minimally 1.5 and a maximum FDR-corrected p-value of 0.05 were considered to be differentially expressed between the two groups (Dataset S3). Principal component analysis was performed on all protein-coding host genes, which had received at least 1 read in any one of the samples. Overrepresentation of gene ontology (GO) terms and KEGG pathways (Dataset S5) among the differentially regulated genes was evaluated with the functional annotation tool (v6.8) of the DAVID bioinformatics database (https://david.ncifcrf.gov/ (Huang da et al., 2009a, b)). Gene set enrichment analysis (GSEA) was performed for all gene sets in the current (v5.1) release of the Molecular Signature Database, using the v2.2.2 javaGSEA analysis tool provided by the Broad Institute (Subramanian et al., 2005) at http://software.broadinstitute.org/gsea. Dataset S7 lists all significantly enriched gene sets containing the keywords ‘B cell’ or ‘interferon’. Additionally, GSEA was performed for the two hallmark Primary Effusion Lymphoma gene sets described by Klein et al. “KLEIN PRIMARY EFFUSION LYMPHOMA UP” and “KLEIN PRIMARY EFFUSION LYMPHOMA DN” (Klein et al., 2003). To investigate expression of the 1252 genes that were differentially regulated between EBV^+ and $EBV^+/KSHV^+$ huNSG-derived cell lines in PEL and donor-derived LCLs, a dataset containing mean gene expression values from each huNSG or LCL sample and the individual PEL samples was subjected to hierarchical cluster analysis (euclidian distance, single linkage) using Cluster 3.0 and Treeview

(v1.1.6r4) (de Hoon et al., 2004; Eisen et al., 1998). Expression values (RPKM) for the individual samples are provided in supplemental Dataset S6.

Human tissue and patient FFPE samples

Studies involving human fetal liver samples as well as peripheral blood samples of healthy volunteers were reviewed and approved by the cantonal ethical committee of Zurich, Switzerland (protocol no. KEK-StV-Nr.19/08). The study of human formalin fixed paraffin embedded (FFPE) samples for research purposes was approved by the Scientific Boards of the University Hospital of Ioannina, Greece (protocol no. 8751) for the two cases described previously in (Papoudou-Bai et al., 2015) and of the Chungnam National University School of Medicine, Daejeon, Korea for one case described previously in (Lee et al., 2017). All TMA samples, described previously in (Arvey et al., 2015), were obtained with the approval of the institutional review boards at Weill Cornell Medical College and the AIDS Malignancy Consortium. Research was conducted in accordance with the Declaration of Helsinki.

Author contributions

D.M., N.C., P.R., A.R., A.M. V.L., I.Q., M.H.M.B, C.S. performed the experiments. D.M., C.S., M.A. and R.E.W. designed the Western blotting experiments. H.J.D. contributed the recombinant EBV viruses. A.F., T.F.S. and D.B. contributed the recombinant KSHV viruses. A.P.B., Y-M.L., J-M.K. and E.C. contributed essential clinical samples. J.M. contributed antibodies for viral protein detection. A.Z. and R.C. determined the EBV titers. G.N. interpreted the histological findings. M.S. and A.G. performed and analyzed the transcriptome sequencing. D.M. and C.M. designed the study and wrote the manuscript.

Acknowledgements

We dedicate this article to Prof. Dr. Martin Allday, who sadly passed away during our collaboration on the presented research project. He was an inspiration to us through his profound knowledge of EBV and his friendly and collaborative personality. This study was supported by Cancer Research Switzerland (KFS-3234-08-2013), Worldwide Cancer Research (14-1033), SPARKS (15UOZ01), $KFSP^{MS}$ and $KFSP^{HHLD}$ of the University of Zurich, the Sobek Foundation, the Swiss Vaccine Research Institute and the Swiss National Science Foundation (310030_162560 and CRSII3_160708) to CM. Donal McHugh is supported by an MD-PhD fellowship from the Swiss National Science Foundation (323530_145247). Thomas F. Schulz is supported by the DFG Collaborative Research Centre 900, project C1. The authors declare no conflict of interest. The authors would like to thank Silvia Behnke of Sophistolab AG, Switzerland for the LANA/LMP1 co-staining performed in Fig. 2B.

REFERENCES

Altmann, M., and Hammerschmidt, W. (2005). Epstein-Barr virus provides a new paradigm: a requirement for the immediate inhibition of apoptosis. PLoS Biol *3*, e404.

Ambroziak, J.A., Blackbourn, D.J., Herndier, B.G., Glogau, R.G., Gullett, J.H., McDonald, A.R., Lennette, E.T., and Levy, J.A. (1995). Herpes-like sequences in HIV-infected and uninfected Kaposi's sarcoma patients. Science *268*, 582-583.

Antsiferova, O., Müller, A., Rämer, P., Chijioke, O., Chatterjee, B., Raykova, A., Planas, R., Sospedra, M., Shumilov, A., Tsai, M.H.*, et al.* (2014). Adoptive transfer of EBV specific $CD8^+$ T cell clones can transiently control EBV infection in humanized mice. PLoS Pathog *10*, e1004333.

Arvey, A., Ojesina, A.I., Pedamallu, C.S., Ballon, G., Jung, J., Duke, F., Leoncini, L., De Falco, G., Bressman, E., Tam, W.*, et al.* (2015). The tumor virus landscape of AIDS-related lymphomas. Blood *125*, e14-22.

Babcock, G.J., Decker, L.L., Volk, M., and Thorley-Lawson, D.A. (1998). EBV persistence in memory B cells in vivo. Immunity *9*, 395-404.

Babcock, J.G., Hochberg, D., and Thorley-Lawson, A.D. (2000). The expression pattern of Epstein-Barr virus latent genes in vivo is dependent upon the differentiation stage of the infected B cell. Immunity *13*, 497-506.

Barros, M.H., Hauck, F., Dreyer, J.H., Kempkes, B., and Niedobitek, G. (2013). Macrophage polarisation: an immunohistochemical approach for identifying M1 and M2 macrophages. PLoS ONE *8*, e80908.

Barros, M.H., Vera-Lozada, G., Soares, F.A., Niedobitek, G., and Hassan, R. (2012). Tumor microenvironment composition in pediatric classical Hodgkin lymphoma is modulated by age and Epstein-Barr virus infection. Int J Cancer *131*, 1142-1152.

Blackbourn, D.J., Lennette, E., Klencke, B., Moses, A., Chandran, B., Weinstein, M., Glogau, R.G., Witte, M.H., Way, D.L., Kutzkey, T.*, et al.* (2000). The restricted cellular host range of human herpesvirus 8. Aids *14*, 1123-1133.

Bouvard, V., Baan, R., Straif, K., Grosse, Y., Secretan, B., El Ghissassi, F., Benbrahim-Tallaa, L., Guha, N., Freeman, C., Galichet, L., and Cogliano, V. (2009). A review of human carcinogens-Part B: biological agents. Lancet Oncol *10*, 321-322.

Brinkmann, M.M., Glenn, M., Rainbow, L., Kieser, A., Henke-Gendo, C., and Schulz, T.F. (2003). Activation of mitogen-activated protein kinase and NF-kappaB pathways by a Kaposi's sarcoma-associated herpesvirus K15 membrane protein. J Virol *77*, 9346-9358.

Bubman, D., Guasparri, I., and Cesarman, E. (2007). Deregulation of c-Myc in primary effusion lymphoma by Kaposi's sarcoma herpesvirus latency-associated nuclear antigen. Oncogene *26*, 4979-4986.

Cannon, J.S., Ciufo, D., Hawkins, A.L., Griffin, C.A., Borowitz, M.J., Hayward, G.S., and Ambinder, R.F. (2000). A new primary effusion lymphoma-derived cell line yields a highly infectious Kaposi's sarcoma herpesvirus-containing supernatant. J Virol *74*, 10187-10193.

Carbone, A., Gloghini, A., Larocca, L.M., Capello, D., Pierconti, F., Canzonieri, V., Tirelli, U., Dalla-Favera, R., and Gaidano, G. (2001). Expression profile of MUM1/IRF4, BCL-6, and CD138/syndecan-1 defines novel histogenetic subsets of human immunodeficiency virus-related lymphomas. Blood *97*, 744-751.

Cesarman, E. (2014). Gammaherpesviruses and lymphoproliferative disorders. Annu Rev Pathol *9*, 349-372.

Cesarman, E., Chang, Y., Moore, P.S., Said, J.W., and Knowles, D.M. (1995). Kaposi's sarcoma-associated herpesvirus-like DNA sequences in AIDS-related body-cavity-based lymphomas. N Engl J Med *332*, 1186-1191.

Chang, Y., Cesarman, E., Pessin, M.S., Lee, F., Culpepper, J., Knowles, D.M., and Moore, P.S. (1994). Identification of herpesvirus-like DNA sequences in AIDS-associated Kaposi's sarcoma. Science *266*, 1865-1869.

Chijioke, O., Muller, A., Feederle, R., Barros, M.H., Krieg, C., Emmel, V., Marcenaro, E., Leung, C.S., Antsiferova, O., Landtwing, V.*, et al.* (2013). Human natural killer cells prevent infectious mononucleosis features by targeting lytic Epstein-Barr virus infection. Cell Rep *5*, 1489-1498.

Cohen, J.I., Fauci, A.S., Varmus, H., and Nabel, G.J. (2011). Epstein-Barr virus: an important vaccine target for cancer prevention. Sci Transl Med *3*, 107fs107.

de Hoon, M.J., Imoto, S., Nolan, J., and Miyano, S. (2004). Open source clustering software. Bioinformatics *20*, 1453-1454.

Eisen, M.B., Spellman, P.T., Brown, P.O., and Botstein, D. (1998). Cluster analysis and display of genome-wide expression patterns. Proc Natl Acad Sci U S A *95*, 14863-14868.

Fan, W., Bubman, D., Chadburn, A., Harrington, W.J., Jr., Cesarman, E., and Knowles, D.M. (2005). Distinct subsets of primary effusion lymphoma can be identified based on their cellular gene expression profile and viral association. J Virol *79*, 1244-1251.

Feederle, R., Kost, M., Baumann, M., Janz, A., Drouet, E., Hammerschmidt, W., and Delecluse, H.J. (2000). The Epstein-Barr virus lytic program is controlled by the co-operative functions of two transactivators. Embo J *19*, 3080-3089.

Friborg, J., Jr., Kong, W., Hottiger, M.O., and Nabel, G.J. (1999). p53 inhibition by the LANA protein of KSHV protects against cell death. Nature *402*, 889-894.

Ganem, D. (2006). KSHV infection and the pathogenesis of Kaposi's sarcoma. Annu Rev Pathol *1*, 273-296.

Godden-Kent, D., Talbot, S.J., Boshoff, C., Chang, Y., Moore, P., Weiss, R.A., and Mittnacht, S. (1997). The cyclin encoded by Kaposi's sarcoma-associated herpesvirus stimulates cdk6 to phosphorylate the retinoblastoma protein and histone H1. J Virol *71*, 4193-4198.

Guasparri, I., Wu, H., and Cesarman, E. (2006). The KSHV oncoprotein vFLIP contains a TRAF-interacting motif and requires TRAF2 and TRAF3 for signalling. EMBO Rep *7*, 114-119.

Hong, G.K., Gulley, M.L., Feng, W.H., Delecluse, H.J., Holley-Guthrie, E., and Kenney, S.C. (2005). Epstein-Barr virus lytic infection contributes to lymphoproliferative disease in a SCID mouse model. J Virol *79*, 13993-14003.

Horenstein, M.G., Nador, R.G., Chadburn, A., Hyjek, E.M., Inghirami, G., Knowles, D.M., and Cesarman, E. (1997). Epstein-Barr virus latent gene expression in primary effusion lymphomas containing Kaposi's sarcoma-associated herpesvirus/human herpesvirus-8. Blood *90*, 1186-1191.

Huang da, W., Sherman, B.T., and Lempicki, R.A. (2009a). Bioinformatics enrichment tools: paths toward the comprehensive functional analysis of large gene lists. Nucleic Acids Res *37*, 1-13.

Huang da, W., Sherman, B.T., and Lempicki, R.A. (2009b). Systematic and integrative analysis of large gene lists using DAVID bioinformatics resources. Nat Protoc *4*, 44-57.

Jenner, R.G., Maillard, K., Cattini, N., Weiss, R.A., Boshoff, C., Wooster, R., and Kellam, P. (2003). Kaposi's sarcoma-associated herpesvirus-infected primary effusion lymphoma has a plasma cell gene expression profile. Proc Natl Acad Sci U S A *100*, 10399-10404.

Kanakry, J., and Ambinder, R. (2015). The Biology and Clinical Utility of EBV Monitoring in Blood. Curr Top Microbiol Immunol *391*, 475-499.

Klein, E., Nagy, N., and Rasul, A.E. (2013). EBV genome carrying B lymphocytes that express the nuclear protein EBNA-2 but not LMP-1: Type IIb latency. Oncoimmunology *2*, e23035.

Klein, U., Gloghini, A., Gaidano, G., Chadburn, A., Cesarman, E., Dalla-Favera, R., and Carbone, A. (2003). Gene expression profile analysis of AIDS-related primary effusion lymphoma (PEL) suggests a plasmablastic derivation and identifies PEL-specific transcripts. Blood *101*, 4115-4121.

Kliche, S., Kremmer, E., Hammerschmidt, W., Koszinowski, U., and Haas, J. (1998). Persistent infection of Epstein-Barr virus-positive B lymphocytes by human herpesvirus 8. J Virol *72*, 8143-8149.

Laichalk, L.L., and Thorley-Lawson, D.A. (2005). Terminal differentiation into plasma cells initiates the replicative cycle of Epstein-Barr virus in vivo. J Virol *79*, 1296-1307.

Lee, Y.M., Kim, J.M., and Kim, S.Y. (2017). Human Herpes Virus 8/Epstein-Barr Virus–Copositive, Plasmablastic Microlymphoma Arising in Multicentric Castleman's Disease of an Immunocompetent Patient. J Path Trans Med *51*, 99-102.

Li, M., Lee, H., Yoon, D.W., Albrecht, J.C., Fleckenstein, B., Neipel, F., and Jung, J.U. (1997). Kaposi's sarcoma-associated herpesvirus encodes a functional cyclin. J Virol *71*, 1984-1991.

Ma, S.D., Hegde, S., Young, K.H., Sullivan, R., Rajesh, D., Zhou, Y., Jankowska-Gan, E., Burlingham, W.J., Sun, X., Gulley, M.L.*, et al.* (2011). A new model of Epstein-Barr virus infection reveals an important role for early lytic viral protein expression in the development of lymphomas. J Virol *85*, 165-177.

Ma, S.D., Yu, X., Mertz, J.E., Gumperz, J.E., Reinheim, E., Zhou, Y., Tang, W., Burlingham, W.J., Gulley, M.L., and Kenney, S.C. (2012). An Epstein-Barr Virus (EBV) mutant with enhanced BZLF1 expression causes lymphomas with abortive lytic EBV infection in a humanized mouse model. J Virol *86*, 7976-7987.

Martin, D.F., Kuppermann, B.D., Wolitz, R.A., Palestine, A.G., Li, H., and Robinson, C.A. (1999). Oral ganciclovir for patients with cytomegalovirus retinitis treated with a ganciclovir implant. Roche Ganciclovir Study Group. N Engl J Med *340*, 1063-1070.

Meyer, M., Hols, A.K., Liersch, B., Leistner, R., Gellert, K., Schalke, B., Marx, A., and Niedobitek, G. (2011). Lack of evidence for Epstein-Barr virus infection in myasthenia gravis thymus. Ann Neurol *70*, 515-518.

Moore, P.S., Boshoff, C., Weiss, R.A., and Chang, Y. (1996). Molecular mimicry of human cytokine and cytokine response pathway genes by KSHV. Science *274*, 1739-1744.

Oksenhendler, E., Boulanger, E., Galicier, L., Du, M.Q., Dupin, N., Diss, T.C., Hamoudi, R., Daniel, M.T., Agbalika, F., Boshoff, C.*, et al.* (2002). High incidence of Kaposi sarcoma-associated herpesvirus-related non-Hodgkin lymphoma in patients with HIV infection and multicentric Castleman disease. Blood *99*, 2331-2336.

Papoudou-Bai, A., Hatzimichael, E., Kyriazopoulou, L., Briasoulis, E., and Kanavaros, P. (2015). Rare variants in the spectrum of human herpesvirus 8/Epstein-Barr virus–copositive lymphoproliferations. Hum Pathol *46*, 1566–1571.

Parkin, D.M. (2006). The global health burden of infection-associated cancers in the year 2002. Int J Cancer *118*, 3030-3044.

Ray, A., and Dittel, B.N. (2010). Isolation of mouse peritoneal cavity cells. J Vis Exp.

Sharp, T.V., Wang, H.W., Koumi, A., Hollyman, D., Endo, Y., Ye, H., Du, M.Q., and Boshoff, C. (2002). K15 protein of Kaposi's sarcoma-associated herpesvirus is latently expressed and binds to HAX-1, a protein with antiapoptotic function. J Virol *76*, 802-816.

Sin, S.H., and Dittmer, D.P. (2013). Viral latency locus augments B-cell response in vivo to induce chronic marginal zone enlargement, plasma cell hyperplasia, and lymphoma. Blood *121*, 2952-2963.

Sin, S.H., Kim, Y., Eason, A., and Dittmer, D.P. (2015). KSHV Latency Locus Cooperates with Myc to Drive Lymphoma in Mice. PLoS Pathog *11*, e1005135.

Soulier, J., Grollet, L., Oksenhendler, E., Cacoub, P., Cazals-Hatem, D., Babinet, P., d'Agay, M.F., Clauvel, J.P., Raphael, M., Degos, L., and et al. (1995). Kaposi's sarcoma-associated herpesvirus-like DNA sequences in multicentric Castleman's disease. Blood *86*, 1276-1280.

Steinbruck, L., Gustems, M., Medele, S., Schulz, T.F., Lutter, D., and Hammerschmidt, W. (2015). K1 and K15 of Kaposi's Sarcoma-Associated Herpesvirus Are Partial Functional Homologues of Latent Membrane Protein 2A of Epstein-Barr Virus. J Virol *89*, 7248-7261.

Strowig, T., Gurer, C., Ploss, A., Liu, Y.F., Arrey, F., Sashihara, J., Koo, G., Rice, C.M., Young, J.W., Chadburn, A.*, et al.* (2009). Priming of protective T cell responses against virus-induced tumors in mice with human immune system components. J Exp Med *206*, 1423-1434.

Subramanian, A., Tamayo, P., Mootha, V.K., Mukherjee, S., Ebert, B.L., Gillette, M.A., Paulovich, A., Pomeroy, S.L., Golub, T.R., Lander, E.S., and Mesirov, J.P. (2005). Gene set enrichment analysis: a knowledge-based approach for interpreting genome-wide expression profiles. Proc Natl Acad Sci U S A *102*, 15545-15550.

Taylor, G.S., Long, H.M., Brooks, J.M., Rickinson, A.B., and Hislop, A.D. (2015). The immunology of Epstein-Barr virus-induced disease. Annu Rev Immunol *33*, 787-821.

Tsai, M.H., Lin, X., Shumilov, A., Bernhardt, K., Feederle, R., Poirey, R., Kopp-Schneider, A., Pereira, B., Almeida, R., and Delecluse, H.J. (2017). The biological properties of different Epstein-Barr virus strains explain their association with various types of cancers. Oncotarget *8*, 10238-10254.

van Esser, J.W., Niesters, H.G., van der Holt, B., Meijer, E., Osterhaus, A.D., Gratama, J.W., Verdonck, L.F., Lowenberg, B., and Cornelissen, J.J. (2002). Prevention of Epstein-Barr virus-lymphoproliferative disease by molecular monitoring and preemptive rituximab in high-risk patients after allogeneic stem cell transplantation. Blood *99*, 4364-4369.

van Esser, J.W., van der Holt, B., Meijer, E., Niesters, H.G., Trenschel, R., Thijsen, S.F., van Loon, A.M., Frassoni, F., Bacigalupo, A., Schaefer, U.W.*, et al.* (2001). Epstein-Barr virus (EBV) reactivation is a frequent event after

allogeneic stem cell transplantation (SCT) and quantitatively predicts EBV-lymphoproliferative disease following T-cell--depleted SCT. Blood *98*, 972-978.

Vieira, J., and O'Hearn, P.M. (2004). Use of the red fluorescent protein as a marker of Kaposi's sarcoma-associated herpesvirus lytic gene expression. Virology *325*, 225-240.

Vom Berg, J., Vrohlings, M., Haller, S., Haimovici, A., Kulig, P., Sledzinska, A., Weller, M., and Becher, B. (2013). Intratumoral IL-12 combined with CTLA-4 blockade elicits T cell-mediated glioma rejection. J Exp Med *210*, 2803-2811.

Wang, L.X., Kang, G., Kumar, P., Lu, W., Li, Y., Zhou, Y., Li, Q., and Wood, C. (2014). Humanized-BLT mouse model of Kaposi's sarcoma-associated herpesvirus infection. Proc Natl Acad Sci U S A *111*, 3146-3151.

White, R.E., Ramer, P.C., Naresh, K.N., Meixlsperger, S., Pinaud, L., Rooney, C., Savoldo, B., Coutinho, R., Bodor, C., Gribben, J.*, et al.* (2012). EBNA3B-deficient EBV promotes B cell lymphomagenesis in humanized mice and is found in human tumors. J Clin Invest *122*, 1487-1502.

Woellmer, A., Arteaga-Salas, J.M., and Hammerschmidt, W. (2012). BZLF1 Governs CpG-Methylated Chromatin of Epstein-Barr Virus Reversing Epigenetic Repression. PLoS Pathog *8*, e1002902.

FIGURE LEGENDS

Figure 1. KSHV persists more frequently in the presence of EBV in huNSG mice and enhances tumor formation.

A) Survival of mice infected with either KSHV (n=14), EBV (n=31) or EBV+KSHV (n=25) or mock infected (n=22) until termination due to >15% weight loss accompanied by general health symptoms. Log-rank test, p=0.024 for EBV vs. EBV+KSHV. **B)** Representative pictures of spleens and one large peritoneal tumor from mice infected with KSHV, EBV (4/25 with 1 tumor and 1/25 with 2 tumors) or EBV+KSHV (6/25 with 1 tumor and 10/25 with 2 tumors) and the frequency of tumor formation observed in huNSG mice. Data pooled from 6 independent experiments, Mann-Whitney test (MWT) for comparison of tumor score, $p<0.001$. **C)** Splenic EBV DNA burden of individual mice infected either with EBV or EBV+KSHV. Median, pooled from 3 independent experiments, MWT, p=0.038. **D)** Splenic KSHV ORF26 DNA burden of individual mice infected either with KSHV or EBV+KSHV, mice without quantifiable levels of ORF26 DNA have been plotted on the x-axis. Median, MWT, p=0.045. Frequency of animals in which KSHV DNA could be detected by qPCR in blood or spleen or both 4 weeks post infection. Pooled from 5 independent experiments, MWT, p=0.016. **E)** Co-staining of LANA or EBNA2 (brown) with CD20 (blue) on representative splenic or tumor sections from infected huNSG. **F)** Frequency of mice infected either with KSHV or EBV+KSHV with or without LANA expression in the spleen. Pooled from 6 independent experiments, two-tailed Fischer's Exact test, p=0.006. **G)** Frequency of $LANA^+$ or $EBNA2^+$ cells with or without CD20 membrane expression in EBV+KSHV or for EBNA2 additionally in EBV infected animals. **H)** Representative histological sections from splenic or tumor sections co-stained with EBNA2 or LANA (brown) and LMP1 (blue). **I)** Frequency of $LANA^+$ or $EBNA2^+$ cells with or without LMP1 membrane expression in EBV+KSHV or for EBNA2 additionally in EBV infected animals. For **G&I)** Mean + SEM, n=4 and 3, respectively **J)** Representative flow cytometric analysis for lineage markers of a terminal peritoneal lavage sample derived from an EBV+KSHV infected huNSG mouse. **K)** Representative flow cytometry plots of

splenocytes stained for *EBER1-2 RNA* with the Quantigene FlowRNA Assay (Affymetrix, Ebioscience) including the control without *EBER1-2* target probe hybridization before the signal amplification procedure and the relative amount of *EBER1-2 RNA*$^+$ cells in each group, mean + SEM. (Mice per group: Mock=3, KSHV=3, EBV=4, EBV+KSHV=5, 3/5 with GFP$^+$ cells). Morphological analysis of H&E stained sections and stratified data of tumor presence in EBV+KSHV infected animals based on KSHV DNA detection in the spleen can be found in the supplemental material (Fig.S1A and S1B respectively).

Figure 2. Tumor cell lines derived from EBV and KSHV dual-infected animals harbor both viruses and exhibit KSHV expression.

A) EBV and KSHV DNA load of representative cell lines expanded ex vivo from EBV or EBV+KSHV infected huNSG mice vs. PEL cell lines. Mean (±SD) of EBV BamHI or KSHV ORF26 copies per cell is depicted including three lines derived from spleen tissues: E9-39, EK7-10 EK3-11, seven from peritoneal lavage samples: E7-13, E7-18, E4-9, E4-3, EK7-8, EK4-2, EK4-11 and two from tumor tissues: E4-9s, EK3-13. **B)** Representative co-stainings of LANA (red) and LMP1 (brown) with blue nuclear counterstain of the EBV$^-$/KSHV$^-$ Burkitt lymphoma cell line Ramos and the two huNSG derived cell lines E3-4 and EK3-13 (EBV$^+$ and EBV$^+$/KSHV$^+$, respectively) with or without the primary antibodies. **C)** Coverage plots of RNA-seq reads mapped to the forward (blue) or reverse (red) strands of the KSHV genome (depicted schematically below) of 3 cell lines derived from dually infected huNSG mice (EK 4-11, 3-11, 3-13) compared to 5 PEL cell lines (KSHV$^+$/EBV$^-$: BCBL1 and AP3; KSHV$^+$/EBV$^+$: AP2, AP5 and HBL6). Numbers in parentheses underneath sample names indicate y-axis scale. As most reads originate from the highly transcribed non-coding RNA pan, plots within each panel are scaled to 10% of maximum genome coverage to allow visualization of transcription across the remainder of the genome. **D)** Hierarchical cluster analysis of the five PEL lines (1 replicate each), and three EBV$^+$/KSHV$^+$ mouse derived cell lines (3 biological replicates each for EK4-11 and EK3-11, 2 replicates for EK3-13) based on mapped

reads to the open reading frames of the KSHV genome. See also Figure S1 and Datasets S1 and S2.

Figure 3. EBV and KSHV dual-positive tumor cell lines show hallmarks of PEL and plasma cell differentiation.

A) Volcano plot of up- and down-regulated host genes in $EBV^+/KSHV^+$ relative to EBV^+ huNSG derived cell lines. All protein-coding host genes, which had received at least 1 read in any one of the samples, were included. Thresholds for differentially regulated genes were an FDR-corrected p-value of 0.05 and an absolute fold change of 1.5. **B)** Principal component analysis of individual biological replicates from EBV^+ (3 replicates each for E4-3 and E4-9) and $EBV^+/KSHV^+$ (3 replicates each for EK4-11 and EK3-11, 2 replicates for EK3-13) cell lines. **C)** Representative GO and KEGG pathway terms significantly enriched among genes that were up- (red) or down-regulated (blue) in $EBV^+/KSHV^+$ relative to EBV^+ cell lines. **D)** Hierarchical cluster analysis of five PEL lines ($KSHV^+/EBV^-$: BCBL1 and AP3; $KSHV^+/EBV^+$: AP2, AP5 and HBL6), three in vitro derived EBV infected (LCL1-3), two EBV^+ (E4-9 and E4-3) and three $EBV^+/KSHV^+$ (EK4-11, EK3-11 and EK3-13) mouse derived cell lines. Analysis was performed for all genes which were differentially expressed between EBV^+ and $EBV^+/KSHV^+$ cell lines. See also supplemental Figure S2A for the detailed cluster analysis. **E)** GSEA: heat map depicting expression values for the enriched genes from the gene set “Primary Effusion Lymphoma Up” core enriched genes: 20/50 (40%), p = 0.066, FDR = 0.067 and “Primary Effusion Lymphoma Down”, core enriched genes: 35/52 (67%), p-value < 0.001, FDR = 0.002 for the individual biological replicates from EBV^+ (three replicates each for E4-3 and E4-9) and $EBV^+/KSHV^+$ (three replicates each for EK4-11 and EK3-11, two replicates for EK3-13) huNSG derived cell lines. See also Fig. S2 for the heat map of the enriched genes in the “Plasma cell vs. memory B-cell up” and “Plasma cell vs. memory B-cell down” gene sets. **F)** Representative histograms and quantification of immune phenotyping by flow cytometry for IRF4 (p=0.042), BLIMP1 (p=0.026), CD40 (p=0.022) and CD19 (p=0.034) of EBV^+

and EBV$^+$/KSHV$^+$ cell lines, n=5-8 and 4-5, respectively, mean+SEM, unpaired t test. **G)** Western blot for LANA, BLIMP1 and γ–tubulin in three EBV$^+$/KSHV$^+$, four EBV$^+$ cell lines, three PEL cell lines and the myeloma cell line U266. Quantification of BLIMP1 relative to γTubulin for the huNSG derived cell lines, mean+SEM, MWT, p=0.057. See also Datasets S1, S3-S8 for detailed analysis of host transcriptome.

Figure 4. EBV and KSHV dual-positive tumor cell lines show enhanced EBV lytic gene expression.

A) Coverage plots of RNA-seq reads mapped to the forward (blue) or reverse (red) strands of the EBV genome (depicted schematically below the coverage plots) of cell lines derived from EBV or EBV/KSHV dually infected animals. Numbers in parentheses underneath sample names indicate y-axis scale. Plots within each panel were scaled to 50% of maximum coverage across the EBV genome. Below, an enlarged view of RNA-seq coverage within the EBV BZLF1 locus (nts. 87,903-92,895) is depicted, where plots were scaled to 10% of the maximum RNA-seq coverage observed across the EBV genome in the corresponding sample. See also Dataset S9 for complete EBV gene coverage and differential EBV gene expression. **B)** Mean (±SEM) relative expression of EBV transcripts in EBV$^+$ compared to EBV$^+$/KSHV$^+$ huNSG derived cell lines and EBV$^+$ lines, determined by RT-qPCR, treated with medium or phorbol-12-myristate-13-acetate and sodium butyrate (TPA/NaB). EBV$^+$ vs. EBV$^+$/KSHV$^+$: MWT; Medium vs. NaB/TPA treated EBV$^+$ lines: two-tailed paired t test. *BZLF1-transcript*: p= 0.003 & 0.009; *CpWp-EBNA1-transcript*: p=0.002 & 0.001; *EBNA2-transcript*: p=0.127 & 0.008; *LMP1-transcript*: p=0.548 & 0.029; *LMP2A-transcript*: p=0.691 & 0.001. **C)** Representative flow cytometry plots of EBV$^+$ and EBV$^+$/KSHV$^+$ cell lines immunostained for intracellular BZLF1 and quantification of cell lines positive for BZLF1 protein from each group. Mean (± SEM), p=0.029, MWT. **D)** Western blot for EBV latent and lytic proteins in two EBV$^+$/KSHV$^+$ and four EBV$^+$ huNSG derived cell lines and three PEL cell lines and two controls. LCLzko: LCL derived from infection of B cells with BZLF1-deficient EBV (EBVzko),

LYTIC: induced 293HEK cells carrying the p2089 EBV-BAC. **E)** Relative number of BZLF1$^+$ cells per spleen of individual mice infected with KSHV, EBV, EBV+KSHV or Mock infected (mean±SEM, MWT p= 0.034 and Fischer's exact test for presence vs. absence of BZLF1 in EBV vs EBV+KSHV: p=0.009). **F)** EBV latency pattern based on co-immunohistochemistry for combinations of EBNA1, EBNA2 and LMP1 in mice infected with EBV or EBV+KSHV (n=3 and 4, respectively). See Figure S3 for representative IHC on huNSG spleen sections.

Figure 5. EBV lytic gene expression leads to enhanced tumorigenesis in EBV and KSHV dual-infected mice.

A) Survival of all mice infected with EBVzko (n=13) or EBVzko+KSHV (n=13) until termination due to ≥15% weight loss with concomitant general health symptoms. Log-rank test for EBVzko vs. EBVzko+KSHV, p=0.317. **B)** Frequency of tumor formation observed in huNSG mice after infection with EBVzko (1/13 with 1 tumor), EBVwt (2/12 with 1 tumor and 1/12 with 2 tumors), EBVzko+KSHV (3/13 with 1 tumor) or EBVwt+KSHV (1/5 with 1 tumor and 3/5 with 2 tumors). MWT of tumor score: EBVzko vs. EBVwt, p=0.249; EBVzko vs. EBVzko+KSHV, p=0.305; EBVwt vs. EBVwt+KSHV, p=0.027; EBVzko+KSHV vs. EBVwt+KSHV, p=0.011. **C)** Splenic EBV DNA burden of mice infected with EBVwt or EBVzko with or without dual infection with KSHV. Median, MWT: EBVzko vs. EBVwt, p=0.314; EBVzko vs. EBVzko+KSHV, p=0.959; EBVwt vs. EBVwt+KSHV, p=0.013; EBVzko+KSHV vs. EBVwt+KSHV, p=0.014. **D)** Frequency of mice with LANA expression in spleen sections from huNSG mice infected with EBVwt+KSHV or EBVzko+KSHV. Two-tailed Fischer's exact test, p=0.486. **E)** Splenic KSHV DNA burden of mice infected with EBVwt+KSHV or EBVzko+KSHV. Median, MWT, p=0.477. **B,C&E)** represent pooled data from 4 experiments. Mock and KSHV infected animals did not develop tumors (n=8 and 3 respectively, not shown). **F)** Frequency of animals in which KSHV DNA could be detected by qPCR for ORF26 in blood or spleen or both 4 weeks post infection, MWT, p=0.586. For **D&F)** EBVzko+KSHV infected animals were compared to the control group "EBV(wt)+KSHV" from Fig.

1. For comparison of EBVwt+KSHV to KSHV infected mice see Fig 1D&F. **G)** Non-reconstituted NSG mice were injected i.p. with 10^7 luciferase expressing EBV^+ or $EBV^+/KSHV^+$ huNSG derived cells or with PBS (Mock) and assessed for luciferase activity for 4 weeks. Representative composite images of in vivo growth monitoring with the region of interest (ROI) in red and the mean (±SEM) luciferase activity measured as photon flux (p/s) within the ROI over time. MWT of photon flux at Day 28, p=0.053. Combined spleen and tumor tissue (if present) weight, mean ±SEM, two-tailed unpaired t test with Welch's correction, p=0.091. Pooled data from two independent experiments (Mock n = 7, EBV^+ n = 10, $EBV^+/KSHV^+$ n = 11). See also Fig.S4 for levels of proinflammatory cytokines in the serum of virus infected huNSG mice..

Figure 6. EBV lytic gene expression is elevated in patient-derived EBV and KSHV dual-infected lymphoproliferations.

A) EBER in situ hybridization, LANA, BZLF1, EBV Viral Capsid Antigen (VCA) immunohistochemistry stainings of two EBV and KSHV dually infected lymphoproliferative disease cases. **B)** BZLF1 and VCA immunohistochemistry stainings of two representative tissue microarray sections (TMAs) of EBV positive $BLIMP1^-$ B cell lymphomas (EBV^+ BCL) including a BL and a non-GC DLBCL case. **C)** Quantification of BZLF1 expressing cells (mean +SD) in histopathological sections from EBV and KSHV dually infected lymphomas and lymphoproliferations ($EBV^+/KSHV^+$ BCL) including three PELs, two EBV and KSHV dually infected lymphoproliferations and one multicentric Castleman's disease-associated microlymphoma and EBV^+ BCL including seven non-GC DLBCL, six BL and two unclassifiable BCL with features of DLBCL and BL (BCL-U), MWT, p=0.020 **D)** Quantification of VCA expressing cells (mean +SD) in histopathological sections from $EBV^+/KSHV^+$ BCL and EBV^+ BCL including six non-GC DLBCL, six BL and two BCL-U, MWT, p=0.110. Cases from HIV negative patients are depicted in red, combined from HIV negative and positive patients in black in **C&D)**. Comparison of HIV negative patients for BZLF1: n=3 and 13, respectively, p=0.019 and VCA: n=3 and 12 respectively,

p=0.012, MWT. **E)** TMAs immunostained for BZLF1 and VCA from a GC-type EBV positive DLBCL case with high expression of BLIMP1.

Figure 1

Click here to download Figure figure 1 090517.tif

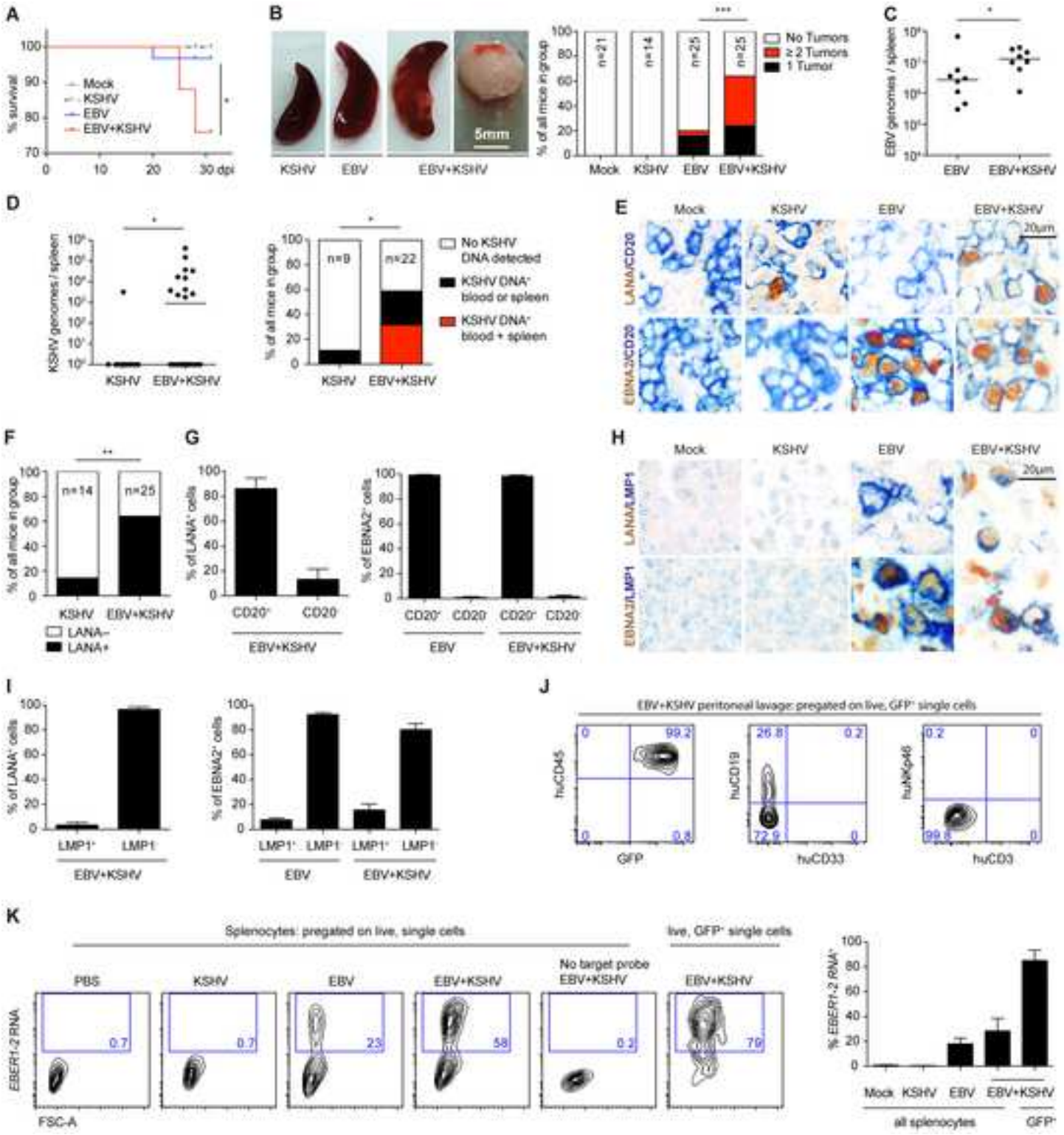

Figure 2

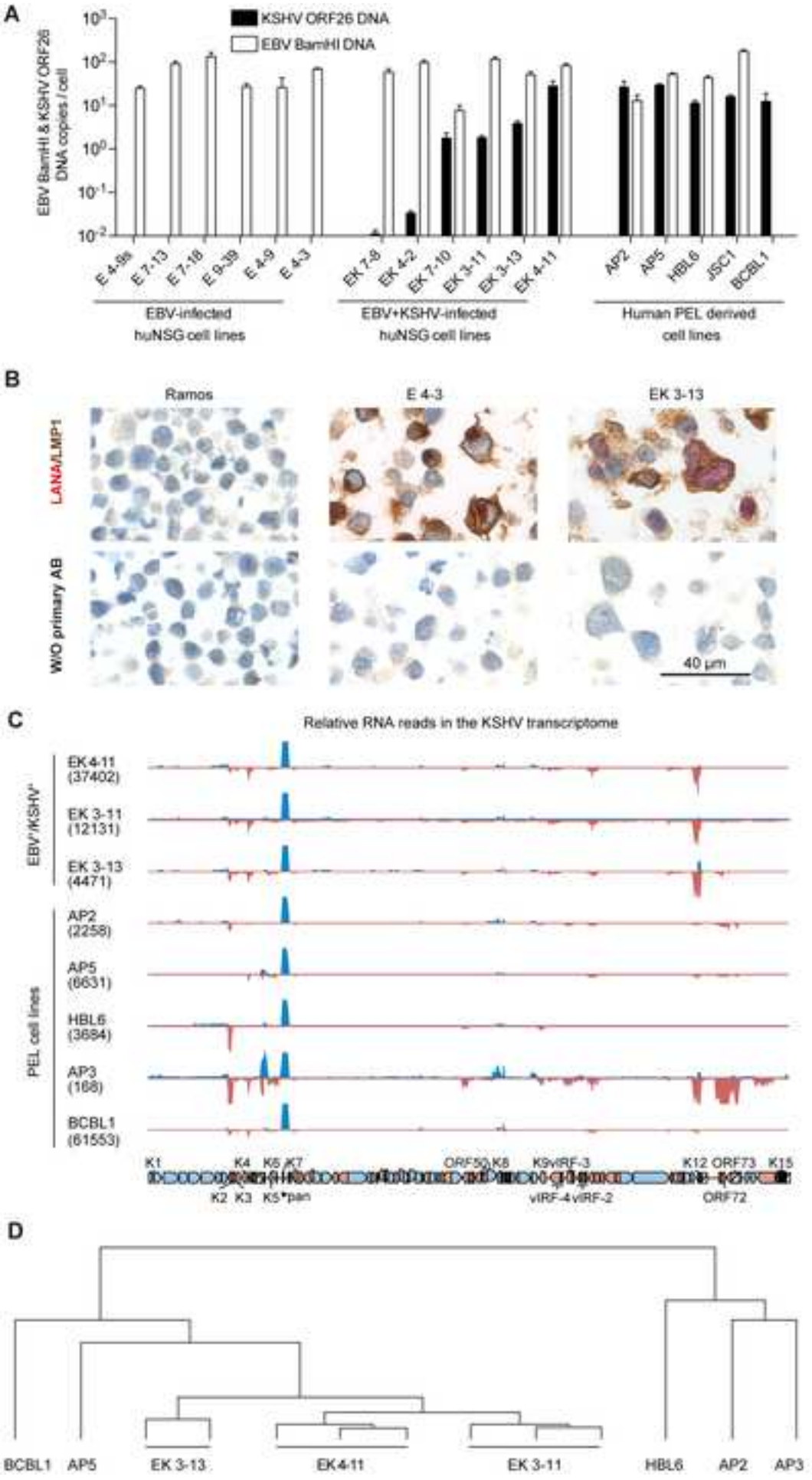

Figure 3

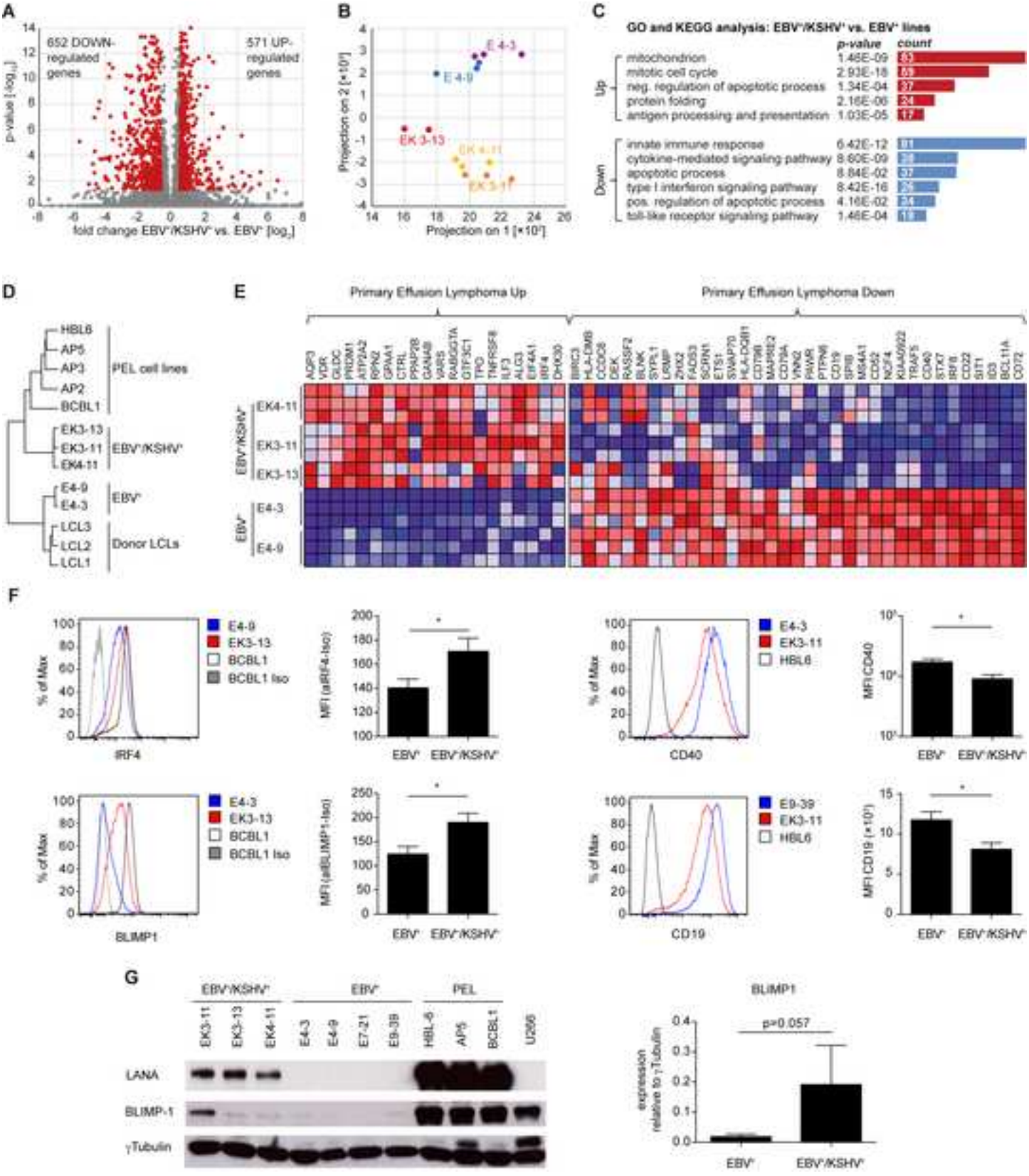

Figure 4

Click here to download Figure figure 4 090517.tif

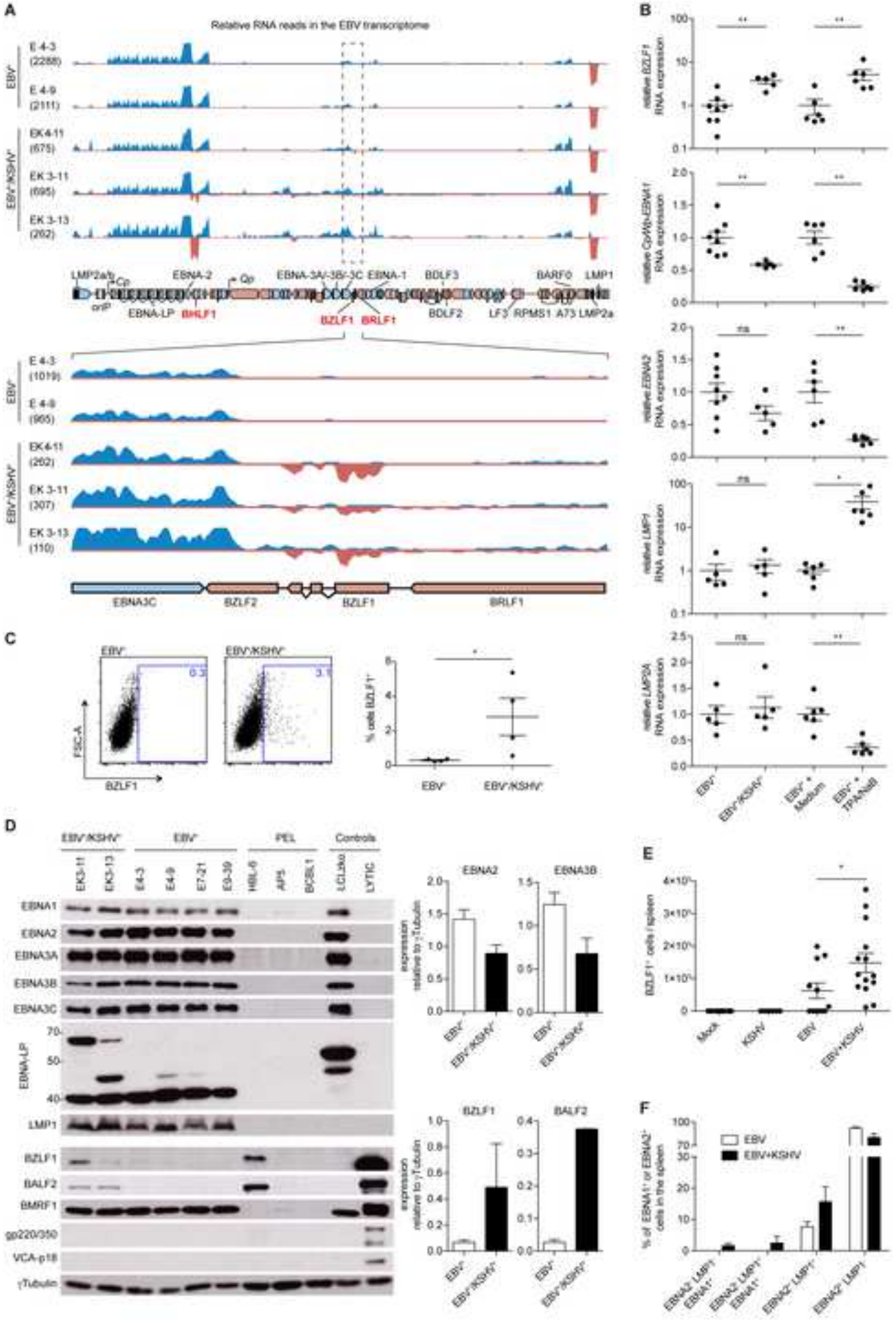

Figure 5

Click here to download Figure figure 5 090517.tif

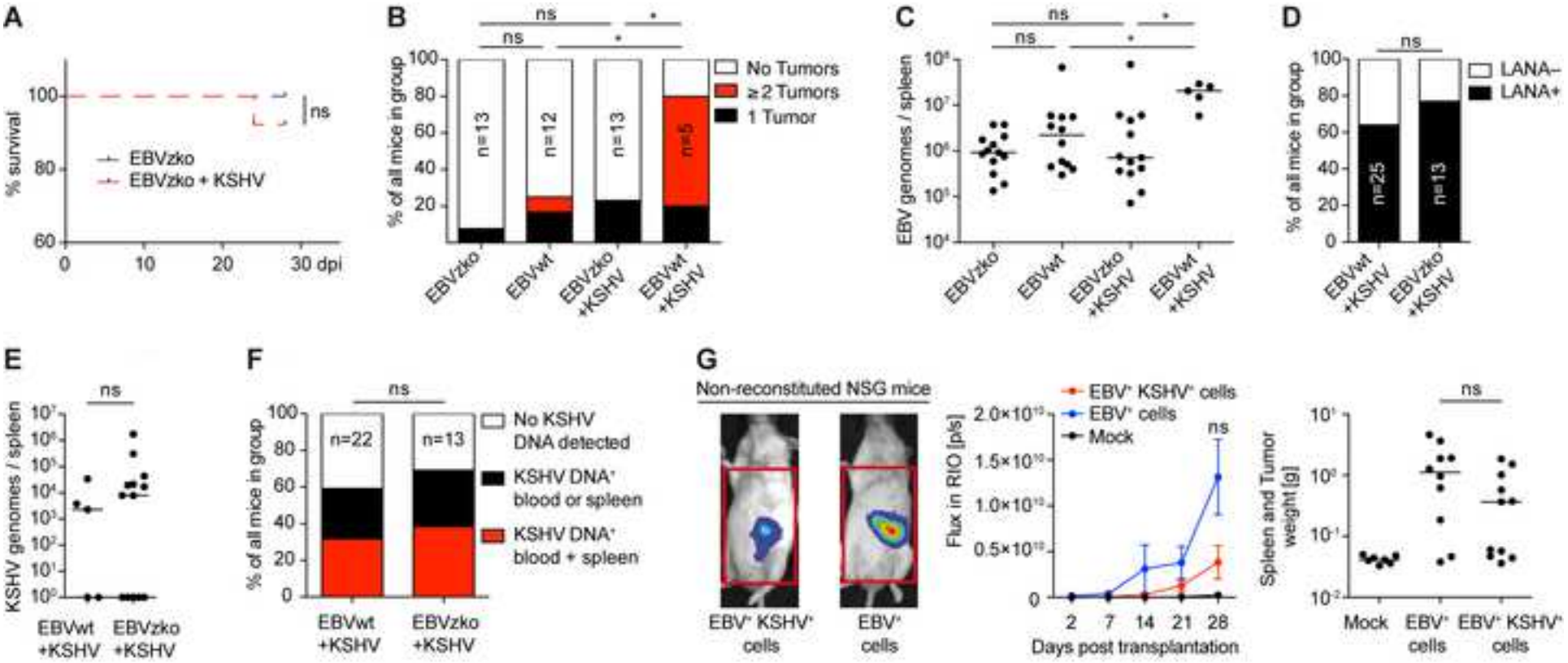

Figure 6

Click here to download Figure figure 6 090517.tif

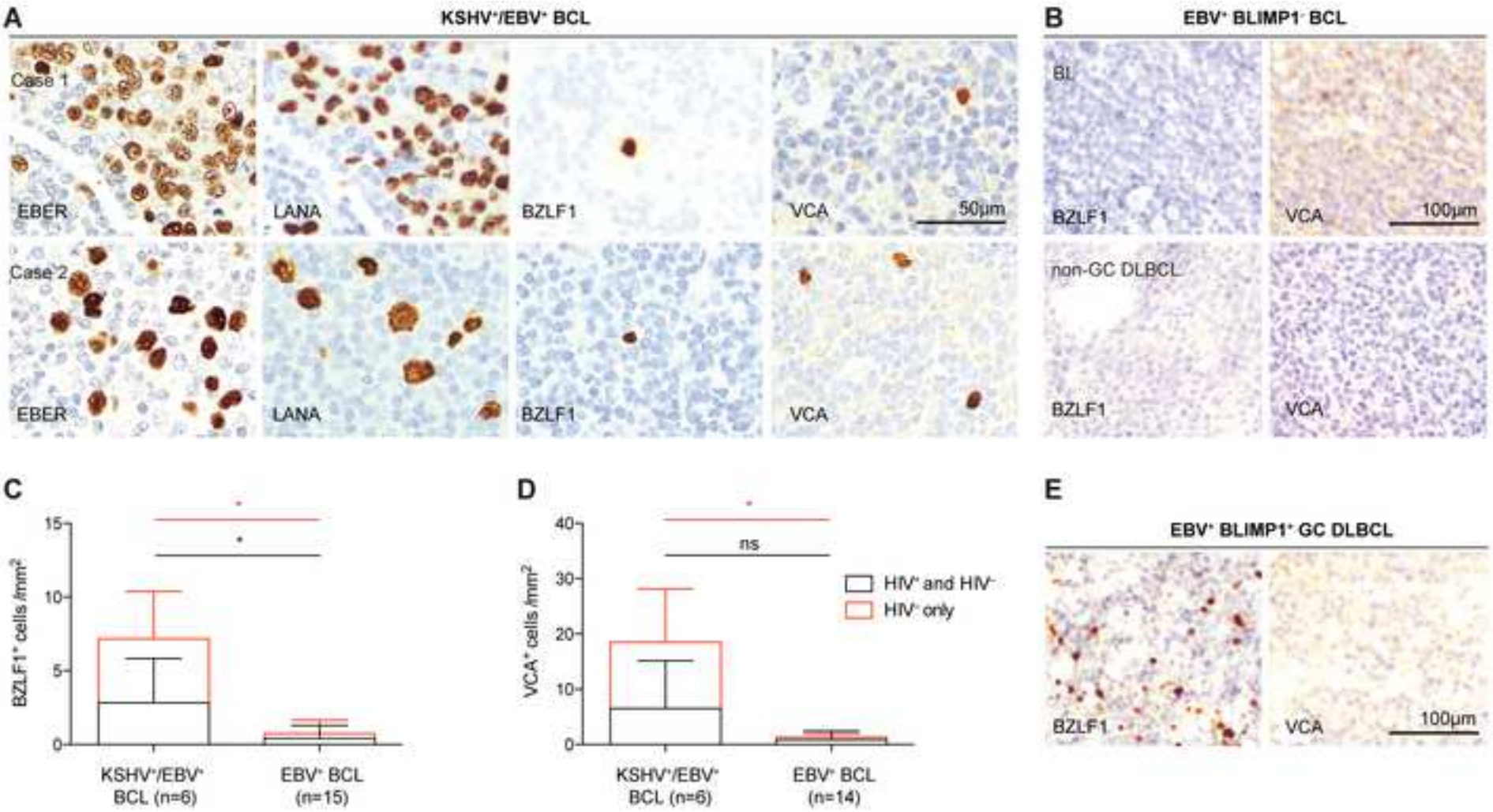

Supplemental Data

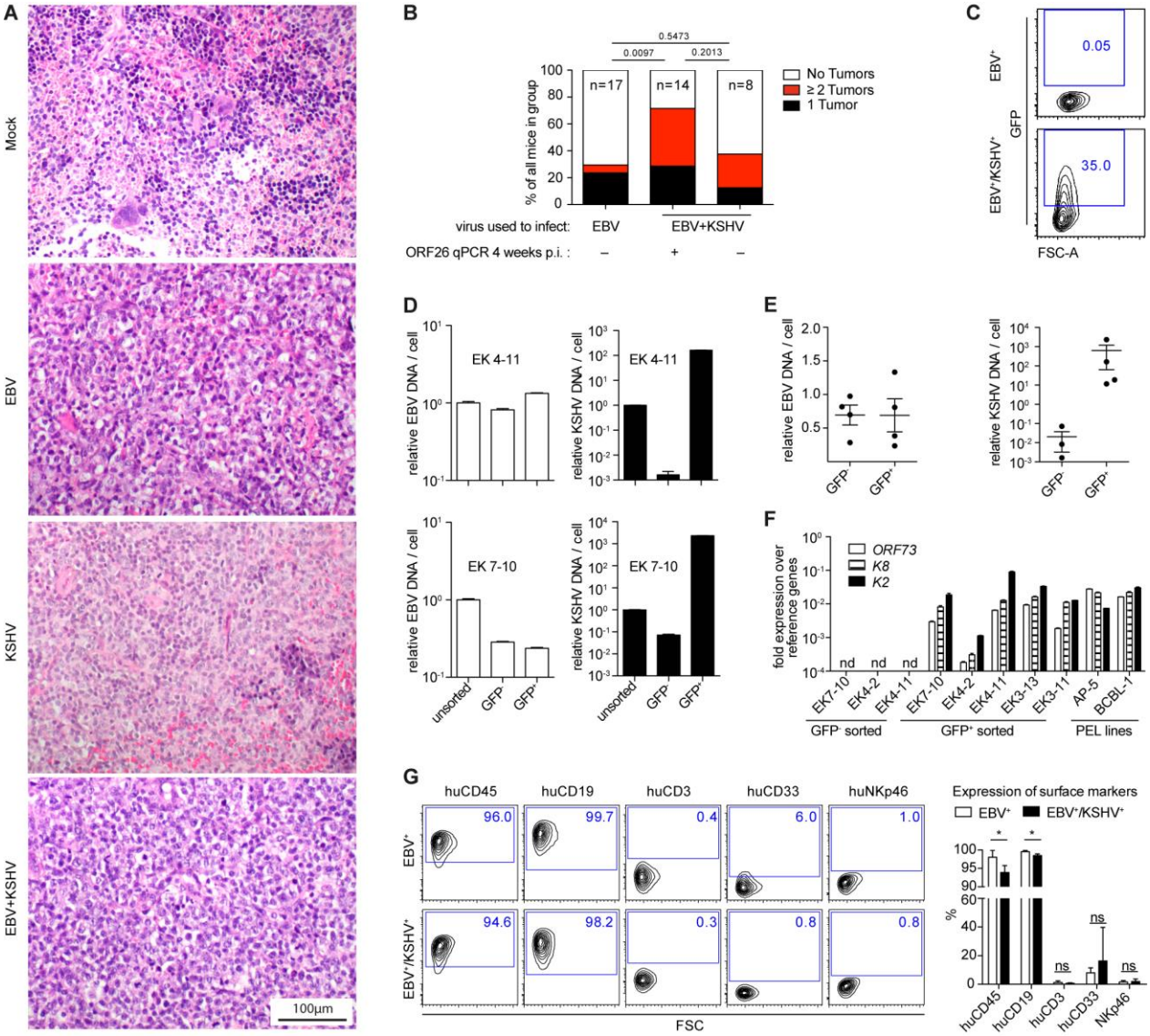

Figure S1, Related to Figure 1&2. Tumor phenotype and frequency in infected huNSG and GFP expression in EBV$^+$/KSHV$^+$ huNSG derived cell lines correlates with KSHV DNA content and KSHV transcription.

A) Representative Hematoxylin/Eosin stainings on splenic sections of huNSG mice infected with KSHV, EBV EBV+KSHV or Mock infected. Formalin-fixed, paraffin embedded tissue sections stained with Hematoxylin and Eosin were examined. In the mock or KSHV infected animals, this revealed the presence of predominantly small to medium-sized lymphoid cells in the white pulp. A small number of central blast-like cells were also observed. No additional pathological changes could be observed in KSHV single-infected compared mock-infected animals. Spleen sections from EBV single infected animals revealed expansion of the white pulp by large lymphoid blasts displaying single or multiple nuclear line and pale cytoplasm, that spilled over into the red pulp. Small areas of necrosis were also observed. Mitotic figures were frequently observed. Similar infiltration by lymphoid blasts was observed at other abdominal sites including peritoneum and pancreas. Histological examination of EBV+KSHV infected animals revealed an identical expansion of the splenic white pulp by lymphoid blast cells. Extensive infiltration at other anatomical sites including small intestinal, pancreas and peritoneum was observed, including areas of geographical necrosis. In conjunction with immunohistochemical phenotype, the infiltration corresponded to diffuse large B cell lymphoma in both EBV single-infected and in EBV+KSHV dually infected animals (see figure 2D for immunohistochemical phenotype).

B) Tumor frequency in EBV and EBV+KSHV infected animals with stratification of the dual infected animals into two groups based on KSHV detection in blood or spleen at 4 weeks post infection. EBV: 4/17 with 1 tumor, 1/17 with 2 or more and 12/17 with no tumors; "EBV+KSHV ORF26^{+}": 4/14 with 1 tumor, 6/14 with 2 or more and 4/12 with no tumors; "EBV+KSHV ORF26^{-}": 1/8 with 1 tumor, 2/8 with 2 or more and 5/8 with no tumors; p-values calculated with MWT.
C) Representative FACS plots from an EBV^{+} and EBV^{+}/KSHV^{+} cell line after pregating on live, single cells.
D) Cell lines were separated into GFP^{+} and GFP^{-} fractions by fluorescence activated cell sorting. Mean (+SD) cellular EBV and KSHV DNA content was determined by qPCR for BamHI and ORF26 respectively and is displayed for the unsorted, GFP^{+} and GFP^{-} fractions of two representative EBV^{+}/KSHV^{+} huNSG derived cell lines relative to the unsorted fraction.
E) A summary of the normalized cellular EBV and KSHV DNA content in GFP^{+} and GFP^{-} sorted fractions from four cell lines is depicted. In one of the GFP^{-} fractions ORF26 could no longer be detected, mean±SEM.
F) Expression of the three KSHV transcripts *ORF73* (LANA), *K8* (K8) and *K2* (viral IL-6) in GFP^{-} and GFP^{+} sorted EBV^{+}/KSHV^{+} huNSG derived cell lines compared to two PEL cell lines (AP5 and BCBL1); nd = not detected, mean+SD.
G) Expression of surface marker on EBV^{+} and EBV^{+}/KSHV^{+} huNSG derived cell lines (n=7 and 4 respectively, mean +SD) with representative plots for EBV^{+} (E4-3) and EBV^{+}/KSHV^{+} (EK3-11) cell lines pre-gated on live single cells. Gates for individual surface markers were determined based on stained donor PBMCs as a positive control. $P<0.05$: *; huCD45: p= 0.023, huCD19: p= 0.017, huCD3: p= 0.315, huCD33: p= 0.788, huNKp46: p= 0.927, MWT.

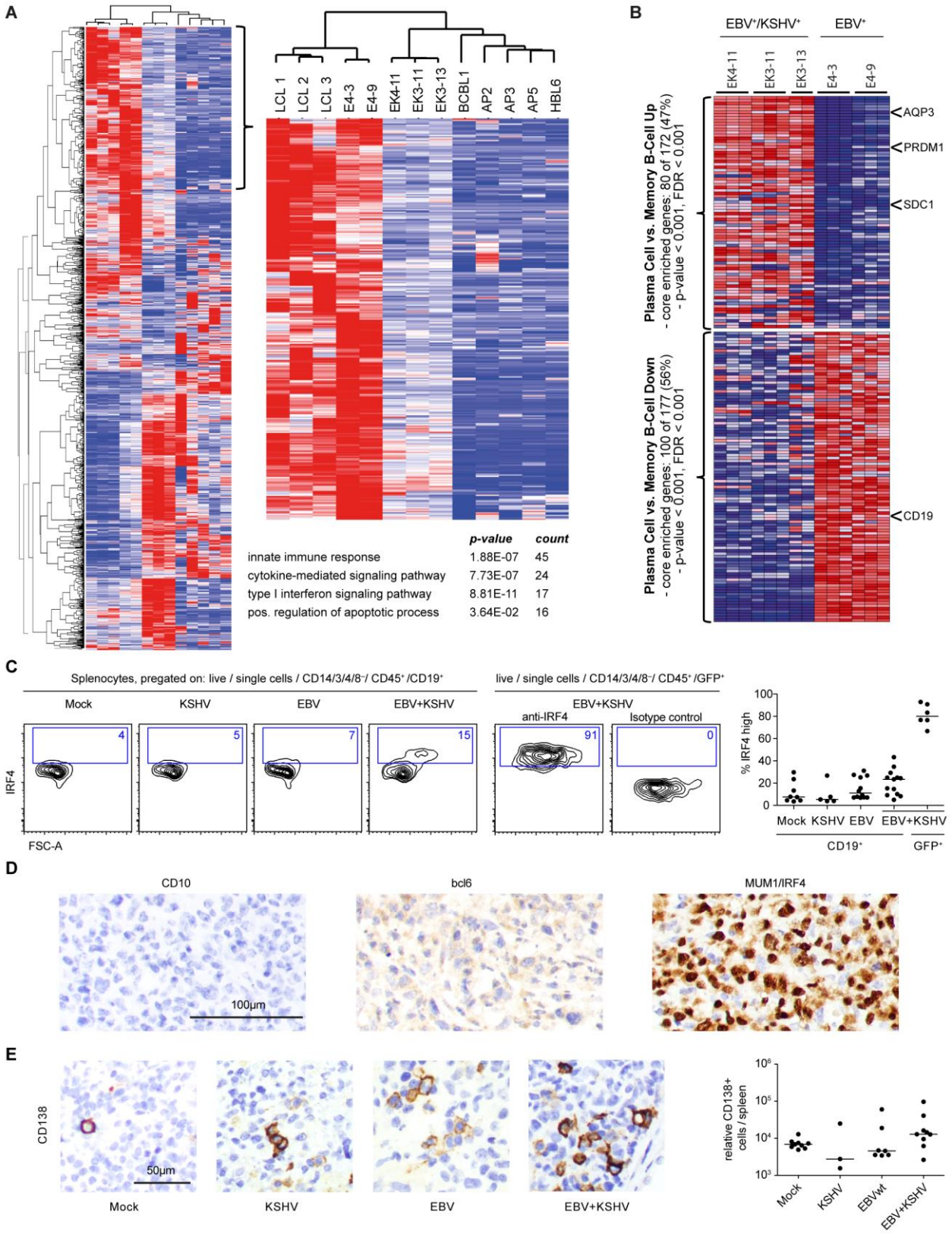
A
LCL 1
LCL 2
LCL 3
E4-3
E4-9
EK4-11
EK3-11
EK3-13
BCBL1
AP2
AP3
AP5
HBL6
p-value count
innate immune response 1.88E-07 45
cytokine-mediated signaling pathway 7.73E-07 24
type I interferon signaling pathway 8.81E-11 17
pos. regulation of apoptotic process 3.64E-02 16
B
EBV+/KSHV+
EBV+
EK4-11
EK3-11
EK3-13
E4-3
E4-9
Plasma Cell vs. Memory B-Cell Up
- core enriched genes: 80 of 172 (47%)
- p-value < 0.001, FDR < 0.001
AQP3
PRDM1
SDC1
Plasma Cell vs. Memory B-Cell Down
- core enriched genes: 100 of 177 (56%)
- p-value < 0.001, FDR < 0.001
CD19
C
Splenocytes, pregated on: live / single cells / CD14/3/4/8-/ CD45+ /CD19+
Mock
KSHV
EBV
EBV+KSHV
IRF4
FSC-A
4
5
7
15
live / single cells / CD14/3/4/8-/ CD45+ /GFP+
EBV+KSHV
anti-IRF4
Isotype control
91
0
% IRF4 high
Mock KSHV EBV EBV+KSHV
CD19+
GFP+
D
CD10
bcl6
MUM1/IRF4
100µm
E
CD138
50µm
Mock
KSHV
EBV
EBV+KSHV
relative CD138+ cells / spleen
Mock
KSHV
EBVwt
EBV+KSHV

Figure S2, Related to Figure 3. Hierarchical clustering of host gene expression, enrichment analysis of Plasma cell vs. memory B-cell gene sets in huNSG derived cell lines and phenotype of infected cells in vivo.
A) Left: Hierarchical cluster analysis of mean host gene expression values in three donor-derived EBV^+ LCLs (LCL1-3), five huNSG mouse derived cell lines (EBV^+: E4-3, E4-9; EBV^+/$KSHV^+$: EK4-11, EK3-11, EK3-13), as well as five primary effusion lymphoma cell lines ($KSHV^+$/EBV^-: BCBL1, AP3; $KSHV^+$/EBV^+: AP2, AP5, HBL6). Analysis was performed for all genes, which were differentially expressed between EBV^+ and EBV^+/$KSHV^+$ huNSG mouse derived cell lines (FDR p value ≤ 0.05, absolute fold change ≥ 1.5). Gene expression values are provided in supplemental dataset S3. Right: Zoomed view of a cluster of genes, which are more highly expressed in EBV^+ compared to EBV^+/$KSHV^+$ huNSG mouse derived cell lines and PELs. Shown below the heat map are representative gene ontology and KEGG pathway terms, which are significantly enriched within this cluster. The complete list of enriched ontology terms is provided in supplemental dataset S6.
B) Heat map depicting expression values for all core enriched genes from the GSE13411 gene sets 'Plasma cell vs. memory B-cell up' (top panel) and 'Plasma cell vs. memory B-cell down' (bottom panel) for the individual biological replicates from EBV^+ (three replicates each for E4-3 and E4-9) and EBV^+/$KSHV^+$ (three replicates each for EK4-11 and EK3-11, two replicates for EK3-13) huNSG derived cell lines. The position of genes encoding for Aquaporin 3 (AQP3), BLIMP1 (PRDM1), CD138 (SDC1) and CD19 (CD19) are indicated on the right. See supplemental dataset S7 for all enriched B-cell and Interferon-related gene sets and S8 for the detailed results of GSEA of the GSE13411 gene sets.
C) Representative flow cytometry plots and quantification of splenocytes from individual mice stained for IRF4 (high) expression in B cells of mice infected with EBV, KSHV or EBV+KSHV or mock-infected and in GFP^+ cells (only in EBV+KSHV infected animals). Pooled data from two independent experiments, median.
D) Representative immunohistochemistry stainings for CD10, bcl6 and IRF4 (=MUM1) on a splenic section of huNSG mouse infected with EBV+KSHV.
E) Representative immunohistochemistry stainings for CD138 on a splenic sections of huNSG mice infected with EBV, KSHV, EBV+KSHV or Mock infected and the quantification of the relative amount of $CD138^+$ cells/ spleen. Pooled from 3 independent experiments, median.

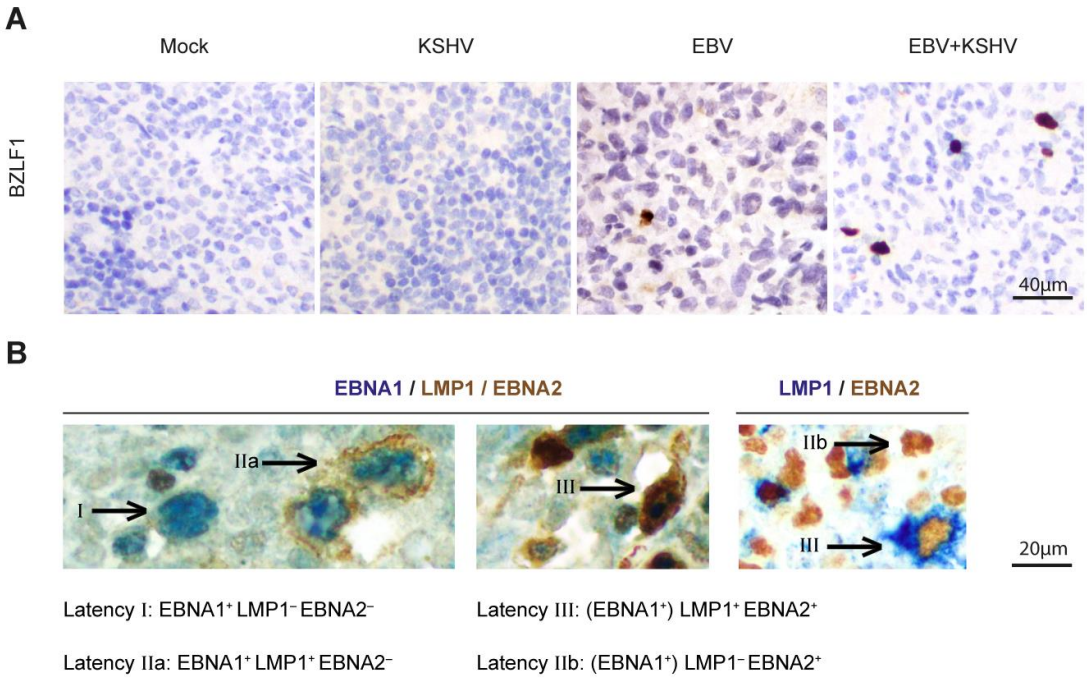

Figure S3, Related to Figure 4. Latent and lytic EBV gene expression in infected huNSG.
A) BZLF1 immunohistochemistry stainings of representative splenic sections from huNSG mice infected with KSHV, EBV, EBV+KSHV or Mock infected.
B) Combined EBNA1/LMP1/EBNA2 immunohistochemistry stainings (left) and LMP1/EBNA2 co-immunohistochemistry stainings (right) of dual infected huNSG mice as a strategy for EBV latency pattern determination in vivo: Sections were stained first for LMP1 and EBNA2 simultaneously using DAB as chromogen. This masked nuclei of all cells showing latencies III or IIb with the brown chromogen and nuclei of cells with latency IIa and latency I remained unstained. Subsequently, sections were stained for EBNA1 using a blue chromogen identifying all cells showing either latency IIa ($LMP1^+/EBNA1^+/EBNA2^-$) or latency I ($EBNA1^+/LMP1^-/EBNA2^-$). For the discrimination between Latency III ($LMP1^+/EBNA2^+$) and Latency IIb ($LMP1^-/EBNA2^+$) separate splenic sections were stained for EBNA2 (brown) and LMP1 (blue).

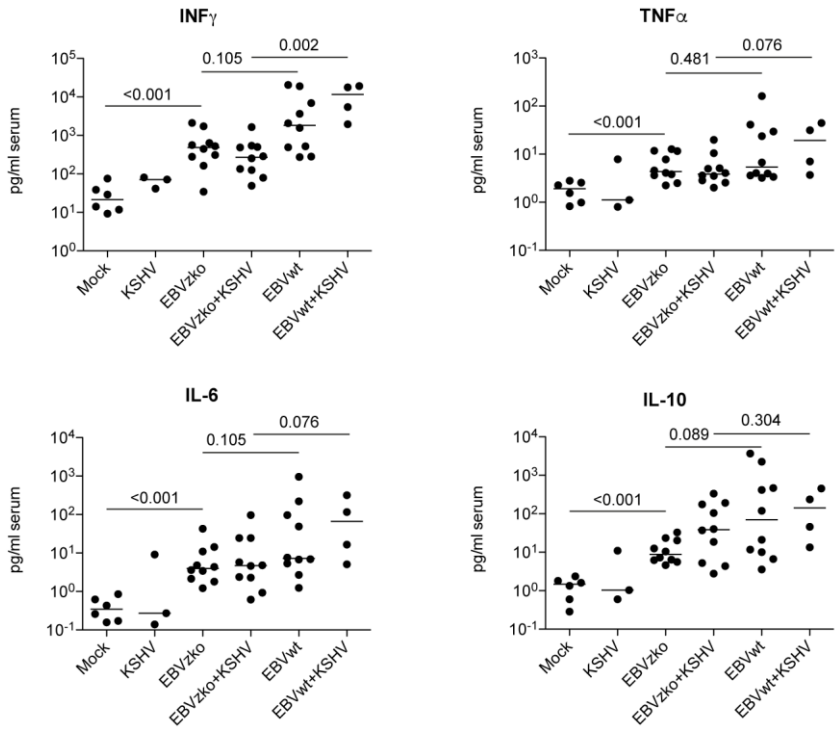

Figure S4, Related to Figure 5. Serum cytokine levels from infected humanized mice.
Serum levels of interferon gamma (IFNγ), tumor necrosis factor alfa (TNFα), Interleukins-6 and -10 (IL-6, -10) were determined at 4 weeks post infection of humanized mice. Data depicted as pg/ml serum for individual animals from each experimental group and the median. Represents pooled data from 3 experiments, p-values calculated with MWT.

Dataset S1, related to Figures 2-4. RNA-seq read statistics.
Left columns show total counts and counts of mapped reads for the individual biological replicates from EBV$^+$ (three replicates each for E4-3 and E4-9) and EBV$^+$/KSHV$^+$ (three replicates each for EK4-11 and EK3-11, two replicates for EK3-13) huNSG derived cell lines. Right columns show counts and percentage (of all mapped reads) of reads which could be mapped to the human genome (assembly hg19), or the genomes of EBV and KSHV genomes (accession numbers NC_007605.1 and NC_009333.1, respectively). Provided as an Excel file.

Dataset S2, related to Figure 2. KSHV RNA-seq coverage and differential gene expression
RNA-seq coverage of forward and reverse strands of the KSHV genome (accession NC_009333.1) in three EBV$^+$/KSHV$^+$ huNSG derived cell lines (three replicates each for EK4-11 and EK3-11, two replicates for EK3-13), two KSHV$^+$/EBV$^-$ PELs (BCBL1, AP3; one replicate each), three KSHV$^+$/EBV$^+$ primary effusion lymphoma cell lines (AP2, AP5, HBL6; one replicate each). Values given for each sample represent the accumulated read coverage across individual replicates. Gene expression in EBV$^+$/KSHV$^+$ huNSG mouse derived cell lines (group MLEK) was compared to that in the five primary effusion cell lines (BCBL1, AP3, AP2, AP5, HBL6) and was based on reads mapped to individual open reading frames (ORFs). Provided as an Excel file.

Dataset S3, related to Figure 3. Differential host gene expression in EBV$^+$ and EBV$^+$/KSHV$^+$ huNSG mouse derived cell lines.
Host gene expression (assembly hg19) in EBV$^+$/KSHV$^+$ huNSG mouse derived cell lines (group MLEK) was compared to that in EBV$^+$ huNSG mouse derived cell lines (group MLE) using the 'RNA-seq' and 'Test on proportions' tools of the CLC workbench (v8.5). Only genes, which had received at least one read in one of the samples, are listed. Provided as an Excel file.

Dataset S4, related to Figure 3. GO-term and KEGG pathway analysis of host genes differentially expressed in EBV$^+$/KSHV$^+$ compared to EBV$^+$ cell lines.
Host genes up- or down-regulated in EBV$^+$/KSHV$^+$ compared to EBV$^+$ huNSG mouse derived cell lines (FDR-corrected p-value <= 0.05, absolute fold change >= 1.5) were subjected to GO/KEGG pathway analysis using the DAVID (v6.8) web server (https://david-d.ncifcrf.gov/). Provided as an Excel file.

Dataset S5, related to Figure 3. Host gene expression in LCLs, huNSG mouse derived cell lines and PEL cell lines.
The dataset lists mean expression values for protein-coding host genes in three donor-derived EBV$^+$ LCLs (LCL1-3), five huNSG mouse derived cell lines (EBV$^+$: E4-3, E4-9; EBV$^+$/KSHV$^+$: EK4-11, EK3-11, EK3-13), as well as five primary effusion lymphoma cell lines (KSHV$^+$/EBV$^-$: BCBL1, AP3; KSHV$^+$/EBV$^+$: AP2, AP5, HBL6). Expression values are shown for all genes, which were differentially expressed between EBV$^+$ and EBV$^+$/KSHV$^+$ positive LCLs (FDR p-value ≤ 0.05, abs. fold change ≥1.5).

Dataset S6, related to Figure 3. GO-term and KEGG pathway analysis of genes more highly expressed in EBV$^+$ compared to EBV$^+$/KSHV$^+$ huNSG mouse derived cell lines and PEL cell lines.
A cluster of genes, which are more highly expressed in EBV$^+$ compared to EBV$^+$/KSHV$^+$ huNSG mouse derived cell lines and PELs (see Supplemental Figure S2) was subjected to GO/KEGG pathway analysis using the DAVID (v6.8) web server (https://david-d.ncifcrf.gov/). Provided as an Excel file.

Dataset S7, related to Figure 3. GSEA of host gene expression in huNSG mouse derived cell lines.
B-cell and Interferon-related gene sets from the Molecular Signature Database (MSigDB, v5.1; http://software.broadinstitute.org/gsea/msigdb/) were compared to gene expression profiles of EBV$^+$/KSHV$^+$ huNSG mouse derived cell lines (group MLEK) and EBV$^+$ huNSG mouse derived cell lines (group MLE) using the javaGSEA analysis tool (http://software.broadinstitute.org/gsea). The tables list all gene sets that were enriched among the MLEK or MLE groups with a nominal p-value of less than 0.05 and an FDR of < 0.2. Provided as an Excel file.

Dataset S8, related to Figure 3. Detailed GSEA results for sets of host genes up or down regulated in plasma vs. memory B cells or in Primary Effusion Lymphoma.
Detailed results from a GSEA (Dataset S7) of EBV$^+$/KSHV$^+$ huNSG mouse derived cell lines (group MLEK) and EBV$^+$ huNSG mouse derived cell lines (group MLE) for two sets of genes that are up- (MSigDB gene set "GSE13411_PLASMA_CELL_VS_MEMORY_BCELL_UP", sheet "PLSM_vs_MEM_UP") or down-regulated (MSigDB gene set "GSE13411_PLASMA_CELL_VS_MEMORY_BCELL_DN", sheet "PLSM_vs_MEM_DN") in plasma vs memory B cells. Detailed results from a GSEA of EBV$^+$/KSHV$^+$ huNSG mouse derived cell lines (group MLEK) and EBV$^+$ huNSG mouse derived cell lines (group MLE) for two sets of genes that are up- (MSigDB gene set "KLEIN_PRIMARY_EFFUSION_LYMPHOMA_UP", sheet "KLEIN_PEL_UP") or down-regulated (MSigDB gene set "KLEIN_PRIMARY_EFFUSION_LYMPHOMA_DN", sheet "KLEIN_PEL_DN") in AIDS-related primary effusion lymphoma (PEL) samples compared to other tumor subtypes and normal B lymphocytes (Klein et al., 2003). Provided as an Excel file.

Dataset S9, related to Figure 4. EBV RNA-seq coverage and gene expression.
RNA-seq coverage of forward and reverse strands of the EBV genome (accession NC_007605.1) in three donor-derived EBV^+ lymphoblastoid cell lines (LCL1-3; three replicates each), two EBV^+ huNSG derived cell lines (E4-3 and E4-9; three replicates each), three $EBV^+/KSHV^+$ huNSG derived cell lines (three replicates each for EK4-11 and EK3-11, two replicates for EK3-13), as well three $KSHV^+/EBV^+$ primary effusion cell lines (AP2, AP5, HBL6; one replicate each). Values given for each sample represent the accumulated read coverage across individual replicates. Gene expression in $EBV^+/KSHV^+$ (group MLEK) and EBV^+ (group MLE) huNSG derived cell lines were compared and was based on reads mapped to individual open reading frames (ORFs). Provided as an Excel file.

Supplemental Experimental Procedures

EBV and KSHV Virus production
Recombinant EBV B95.8 (EBVwt, p2089) and EBV B95.8-deltaBZLF1 (EBVzko) were produced in 293 HEK cells and the titers of virus concentrates (in Raji Infecting Units, RIU) were determined by flow cytometric analysis of GFP positive cells 2 days after infection in vitro as previously described (Antsiferova et al., 2014; Chijioke et al., 2013). Recombinant KSHV (rKSHV.219) was produced as previously described in Vero cells (Vieira and O'Hearn, 2004) or in BrK.219 cells (Kati et al., 2015) and titrated on HEK 293T cells. Infectious units (IU) were determined by flow cytometric analysis of GFP positive cells 2 days after infection on FACSCanto II or LSR Fortessa (BD Biosciences).

Quantification of EBV and KSHV DNA in huNSG spleen and blood
Total DNA from splenic tissue and whole blood was extracted using DNeasy Blood & Tissue Kit (Qiagen) and NucliSENS (bioMérieux), respectively, according to manufacturer's instructions. Quantitative analysis of EBV DNA in huNSG spleens and blood was performed by a TaqMan (Applied Biosystems) real-time PCR as described previously (Berger et al., 2001) with modified primers (5'-CTTCTCAGTCCAGCGCGTTT-3' and 5'-CAGTGGTCCCCCTCCCTAGA-3') and the fluorogenic probe (5'-(FAM)-CGTAAGCCAGACAGCAGCCAATTGTCAG-(TAMRA)-3') for the amplification of a 70-base pair sequence in the conserved BamHI W fragment of EBV. PCR was run on an ABI Prism 7700 Sequence Detector (Applied Biosystems) and sample analyzed in duplicates. KSHV in spleen and blood DNA were determined by quantitative amplification of ORF26 as described below. The presence of KSHV DNA in blood and spleen in KSHV infected and EBV+KSHV dually infected huNSG mice was compared with a PCR score: A score of 1 was awarded for detection in blood or spleen; 2 for detection in blood and spleen; 0 for no detection.

Quantification of EBV and KSHV DNA contents in cell lines
Total DNA was isolated from cell lines with the DNeasy Blood & Tissue Kit (Qiagen) using manufacturer's protocols. KSHV and EBV DNA content was determined by quantitative amplification of KSHV ORF26, EBV BamH1 and the human reference gene BCL-2 using the following primer-probe combinations: BamHI forward primer: 5′-GGACCACTGCCCCTGGTATAA-3′, EBV BamHI reverse primer: 5′-TTTGTGTGGACTCCTGGGG-3′, EBV BamHI probe: 5′-(FAM)-TCCTGCAGCTATTTCTGGTCGCATCA-(TAMRA)-3′, KSHV ORF26 forward primer: 5'-GCTCGAATCCAACGGATTTG-3', KSHV ORF26 reverse primer: 5'-AATAGCGTGCCCCAGTTGC-3, KSHV ORF26 probe 5'-(FAM)-TTCCCCATGGTCGTGCCTC-(BHQ-1)-3' (ORF26 primers and probe modified from (Tedeschi et al., 2001)), BCL-2 forward primer: 5′-CCTGCCCTCCTTCCGC-3′, BCL-2 reverse primer 5′-TGCATTTCAGGAAGACCCTGA-3′, BCL-2 probe 5′-(FAM)-CTTTCTCATGGCTGTCC-(TAMRA)-3′. Real-time PCR amplification was performed using the TaqMan Universal PCR Master Mix (Applied Biosystems) and 250ng DNA extracted from cultured cells on a C1000 Touch CFX384 Real-Time platform (Bio-Rad, Hercules, CA, USA) starting with 2min at 50°C and 10min at 95°C, followed by 50 cycles of amplification (95 °C for 15s, 60 °C for 1min). Cq values were determined with the CFX-manager software (Biorad) using a regression algorithm.

Quantitative reverse transcription PCR for viral gene expression
Total RNA was isolated from cell lines using the RNeasy Mini Kit (Qiagen) according to the recommendations of the manufacturer. To remove contaminating genomic DNA, a 15min on-column DNase treatment was included during RNA isolation (RNase-Free DNase Set, Qiagen). The purified RNA was immediately reverse-transcribed with GoScript Reverse Transcriptase (Promega) according to the manufacturer's recommendations in a 20µl volume for 1h at 42°C using a primer mix combining previously described 3' gene-specific RT primers (Bell et al., 2006) at concentrations of 10µM each. Gene-specific RT primers for SDHA: 5'-TTATGCGATGGATGGACC-3', ORF73: 5'-GTGGATTACCCTGTTGTTA-3', K8: 5'-TACCTTAACTACAGACGCA-3' and K2 5'-TGTGGTCTATCTTGCTGGTA-3' were designed using CLC Main Workbench software (Qiagen). After 15min heat inactivation at 70°C, cDNA was stored at -20°C until qPCR. Amplifications of *Cp/Wp-EBNA1*, *EBNA2*, *LMP1*, *LMP2A* as well as *BZLF1*, *ORF73*, *K8*, *K2*, *GAPDH* and *SDHA* were carried out in triplicate with equal volumes of input RNA and TaqMan universal PCR reagents (Applied Biosystems) using either previously published primer sets with 5'FAM/3'TAMRA (Bechtel et al., 2005; Bell et al., 2006; Krishnan et al., 2004; Sharma-Walia et al., 2005) or 5'FAM/3'MGB labeled probes for SDHA (TaqMan Applied Biosystems Gene Expression Assay (Hs00417200)). Thermal cycling was performed with a C1000 Touch CFX384 Real-Time platform (Bio-Rad) starting with 2min at 50°C and 10min at 95°C, followed by 50 cycles of amplification (95 °C for 15s, 60 °C for 1min). Cq values were determined with the CFX-manager software (Biorad) using a regression algorithm. Transcript levels were calculated relative to the geometric mean of the two reference genes GAPDH and SDHA and then normalized to the mean value of the EBV^+ cell lines.

Flow cytometric analysis of cell lines
PELs and huNSG-derived cell lines were stained for surface markers using conjugated antibodies detecting CD40 (APC, 5C3), CD19 (PE-Cy7, HIB19) and CD138 (APC, MI15), all purchased from Biolegend. To assess cell viability, samples were co-stained with Zombie Aqua Fixable Dye (Biolegend). Intracellular staining assays were performed as previously described for BZLF-1 (Antsiferova et al., 2014). In brief, cells were fixed and permeabilized with the Cytofix/Cytoperm Kit (BD) and stained intracellularly using AF647-labelled rat anti-IRF4 antibody (IRF4.3E4, Biolegend) or mouse anti-ZEBRA (BZ.1, Santa Cruz) primary antibody and secondary goat anti-mouse AF647 antibody (Invitrogen). Intranuclear

staining of BLIMP-1 was performed after fixation and permeabililzation with Foxp3 staining kit reagents (eBioscience) using a AF647-labeled antibody (646702, Novus biological). For intranuclear and intracellular proteins, appropriate isotype control stainings were included and the percent or MFI of positive cells were determined by subtracting the background values (isotype control). Acquisition was performed on FACSCanto II or LSR Fortessa flow cytometer (BD Biosciences) and data was analyzed using FlowJo 9.9 software.

Flow cytometric analysis of splenocytes and peritoneal lavage cells

Peritoneal lavage cells were washed once with PBS and then stained. Single cell suspensions of huNSG-derived splenocytes were subjected to Ficoll gradient centrifucation (Ficoll-Paque Premium,GE Healthcare) before the staining of surface markers using a combination of the following antibodies (purchased from either Biolegend or BD Bioscience): CD45-PB (HI30), CD3-BV510 (UCHT1) or BV785 (OKT3), CD14-BV510 (M5E2), CD4-BV510 (RPA-T4), CD8-PerCp (SK1), CD19-BV785 or PE-Cy7 (HIB19), CD20-APC-Cy7 (2H7), CD33-APC-Cy7 (P67.6), NKp46-APC (9-E2). Live/dead cell discrimination and intracellular IRF4 staining as well as data acquisition and analysis were performed as described in the above section. Flow cytometry RNA staining of EBER1-2 was performed with the Quantigene® FlowRNA Assay (Affymetrix, Ebioscience) according to the manufacturer's recommendations. In brief, cells were stained with Zombie Aqua Fixable dye (Biolegend) prior to a PFA/methanol-based fixation with the buffers provided by the manufacturer and stored at -80° in 100% methanol until use. After fixation and permeabilization, cells were incubated with target probes, specific for EBER1-2 RNA (VF6-12431) followed by signal amplification and labeling with AF647-probes. Samples were acquired on an LSR Fortessa flow cytometer (BD) and analyzed with FlowJo 9.9 software.

Lytic induction of cell lines

EBV lytic gene expression was induced in huNSG-derived cell lines using culture medium (R8) supplemented with 20 ng/mL phorbol-12-myristate-13-acetate (TPA) and 3mM sodium butyrate as previously described (Robinson et al., 2012). After 16h, total RNA was isolated and EBV gene expression was measured by RT-qPCR as described above.

Serum cytokine determination

Serum was collected upon terminal bleeding of animals at 4 weeks post infection and frozen at -80°C until use. Cytokine concentrations in the serum of individual mice were measured in duplicate with the V-PLEX Proinflammatory Panel 1 (Mesoscale K15049D-2) according to the manufacturer's instuctions. Plates were read with a Meso Quickplex SQ120 (Mesoscale) and analyzed with Discovery Workbench® 4.0.12 (Mesoscale). Standard dilutions for the calibrator blend for standard curve generation were performed in quadruplicate.

Western Blotting

Protein analysis was performed by Western blotting essentially as described previously (Anderton et al., 2008)(Kalchschmidt et al., 2016). Briefly, protein was extracted using radioimmunoprecipitation (RIPA) lysis buffer, resolved using SDS polyacrylamide gel electrophoresis (SDS-PAGE) and transferred onto nitrocellulose membranes (Protran). Membranes were then probed with antibodies, as listed in Table 1. U266 cells (Nilsson et al., 1970) used as a control in selected Western blots were obtained from the Flow Cytometry Facility at Hammersmith Hospital (Imperial College London) and were routinely cultured in RPMI 1640 medium (Invitrogen) supplemented with 10% FBS and penicillin-streptomycin at a final concentration of 5 µg/ml.

Triple labeling immunohistochemistry for EBV latency patterns.

Triple labeling immunohistochemistry was performed to evaluate the expression of LMP1 by $EBNA1^{+}EBNA2^{-}$ cells (Latency II pattern), as well as to identify the cells with Latency I pattern ($EBNA1^{+}EBNA2^{-}LMP1^{-}$ cells). For this the antigen retrieval was performed as described for double labelling immunohistochemistry. After incubation with appropriately diluted EBNA2 (clone PE2, kind gift from M. Rowe, Birmingham, UK) primary antibody (30 minutes), immobilized antibody was detected using ZytoChem Plus HRP polymer kit (Zytomed Systems, Berlin, Germany), employing DAB as substrate. Subsequently, slides were washed in Wash Buffer (Zytomed Systems, Berlin, Germany) for 5 minutes and the appropriately diluted LMP1 (clones CS1-4, Zytomed Systems) antibody was incubated for 30 minutes. The immobilized LMP1-antibody was detected using ZytoChem Plus HRP polymer kit (Zytomed Systems, Berlin, Germany), employing again DAB as substrate. This yielded in a brown nuclear and cytoplasmic/membraneous labelling of latency III cells masking nuclei for subsequent staining for EBNA1, and an exclusively cytoplasmic/membraneous brown labelling of latency II cells. Subsequently, the slides were washed in Wash Buffer (Zytomed Systems, Berlin, Germany) for 5 minutes and the appropriately diluted EBNA1 (clone 1H4 kindly provided by Dr. Kremmer, Munich, Germany) antibody was incubated overnight at 4ºC. Following another washing step using Wash Buffer (Zytomed Systems, Berlin, Germany), bound antibody were detected using the AP Polymer System (Zytomed Systems, Berlin, Germany), employing Blue Alkaline Phosphatase (Vector Laboratories, California, USA) as substrate. The sections were not counterstained. This yielded a blue nuclear staining only in latency I and latency II cells, thus allowing the identification of cells expressing EBNA1.

Generation of luciferase lentivirus

Lentivirus containing a firefly luciferase expression cassette was generated as previously described (Schmid et al., 2007) by co-transfecting the calcium-phosphate precipitated plasmids pCMVΔR8.91, pMDG and the lentiviral luciferase expression vector (pLenti CMV V5-LUC Blast (w567-1), addgene) in 293T cells (Campeau et al., 2009). Lentivirus containing cell culture supernatants were harvested 3 days after transfection, filtered through a 0.2 µM filter and used immediately or stored at -80 °C until use.

PEL Cell lines used for High-throughput sequencing and RNA-seq analysis

The primary effusion (PEL) cell lines BCBL1 and HBL6 (Carbone et al., 1998; Renne et al., 1996) were obtained from the laboratory of Don Ganem (University of California, San Francisco). AP2, AP3 and AP5 (Gaidano et al., 1996) cells were obtained from the German Collection of Microorganisms and Cell Cultures (DSMZ; catalogue numbers ACC-48, ACC-275 and ACC-215, respectively). All PELs were cultured in RPMI 1640 medium (Invitrogen) supplemented with 20% FBS and penicillin-streptomycin at a final concentration of 5 µg/ml, and were routinely subjected to PCR testing to ensure absence of mycoplasma contamination (LookOut mycoplasma PCR detection kit, Sigma-Aldrich). The identity of PEL lines was confirmed by high-throughput mRNA sequencing and subsequent analysis of sequence signatures of reads mapping to KSHV genomes in BCBL1 and AP3 cells, or KSHV as well as EBV genomes in co-infected PEL cell lines (HBL6, AP2 and AP5).

Table 1. Western Blot Antibodies

Antibody	Description	Source
anti-EBNA3A	Sheep polyclonal	Abcam, ab16126
anti-EBNA3B	6C9, Rat monoclonal	(White et al., 2010)
anti-EBNA3C	A.10 hybridoma, mouse monclonal	Gift from Prof. M Rowe (Maunders et al., 1994)
anti-EBNA1	Human serum	Gift from Prof. P Farrell
anti-EBNA2	Mouse monoclonal	Abcam, ab90543
anti-EBNA-LP	JF-186, mouse monoclonal	(Finke et al., 1987)
anti-LMP1	Mouse monoclonal	DAKO, CS1-4
anti-γ-tubulin	Mouse monoclonal	Sigma-Aldrich, T6557
anti-LANA	Mouse monoclonal	Sigma-Aldrich, 13B10
anti-BLIMP-1	Rabbit monoclonal	Cell Signalling, C14A4
anti-BZLF1	Mouse monoclonal	Gift from Prof. P Farrell
anti-BALF2	OT13N, Mouse	Provided by J. Middeldorp
anti-gp220/350	OT6, Mouse	Provided by J. Middeldorp
anti-VCA-p18	OT41A, Rabbit	Provided by J. Middeldorp
anti-BMRF1	OT14E, Mouse	Provided by J. Middeldorp

Supplemental References

Anderton, E., Yee, J., Smith, P., Crook, T., White, R.E., and Allday, M.J. (2008). Two Epstein-Barr virus (EBV) oncoproteins cooperate to repress expression of the proapoptotic tumour-suppressor Bim: clues to the pathogenesis of Burkitt's lymphoma. Oncogene *27*, 421-433.

Antsiferova, O., Müller, A., Rämer, P., Chijioke, O., Chatterjee, B., Raykova, A., Planas, R., Sospedra, M., Shumilov, A., Tsai, M.H.*, et al.* (2014). Adoptive transfer of EBV specific $CD8^+$ T cell clones can transiently control EBV infection in humanized mice. PLoS Pathog *10*, e1004333.

Bechtel, J., Grundhoff, A., and Ganem, D. (2005). RNAs in the virion of Kaposi's sarcoma-associated herpesvirus. J Virol *79*, 10138-10146.

Bell, A.I., Groves, K., Kelly, G.L., Croom-Carter, D., Hui, E., Chan, A.T., and Rickinson, A.B. (2006). Analysis of Epstein-Barr virus latent gene expression in endemic Burkitt's lymphoma and nasopharyngeal carcinoma tumour cells by using quantitative real-time PCR assays. J Gen Virol *87*, 2885-2890.

Berger, C., Day, P., Meier, G., Zingg, W., Bossart, W., and Nadal, D. (2001). Dynamics of Epstein-Barr virus DNA levels in serum during EBV-associated disease. J Med Virol *64*, 505-512.

Campeau, E., Ruhl, V.E., Rodier, F., Smith, C.L., Rahmberg, B.L., Fuss, J.O., Campisi, J., Yaswen, P., Cooper, P.K., and Kaufman, P.D. (2009). A versatile viral system for expression and depletion of proteins in mammalian cells. PLoS ONE *4*, e6529.

Carbone, A., Cilia, A.M., Gloghini, A., Capello, D., Todesco, M., Quattrone, S., Volpe, R., and Gaidano, G. (1998). Establishment and characterization of EBV-positive and EBV-negative primary effusion lymphoma cell lines harbouring human herpesvirus type-8. Br J Haematol *102*, 1081-1089.

Chijioke, O., Muller, A., Feederle, R., Barros, M.H., Krieg, C., Emmel, V., Marcenaro, E., Leung, C.S., Antsiferova, O., Landtwing, V.*, et al.* (2013). Human natural killer cells prevent infectious mononucleosis features by targeting lytic Epstein-Barr virus infection. Cell Rep *5*, 1489-1498.

Finke, J., Rowe, M., Kallin, B., Ernberg, I., Rosen, A., Dillner, J., and Klein, G. (1987). Monoclonal and polyclonal antibodies against Epstein-Barr virus nuclear antigen 5 (EBNA-5) detect multiple protein species in Burkitt's lymphoma and lymphoblastoid cell lines. J Virol *61*, 3870-3878.

Gaidano, G., Cechova, K., Chang, Y., Moore, P.S., Knowles, D.M., and Dalla-Favera, R. (1996). Establishment of AIDS-related lymphoma cell lines from lymphomatous effusions. Leukemia *10*, 1237-1240.

Kalchschmidt, J.S., Bashford-Rogers, R., Paschos, K., Gillman, A.C., Styles, C.T., Kellam, P., and Allday, M.J. (2016). Epstein-Barr virus nuclear protein EBNA3C directly induces expression of AID and somatic mutations in B cells. J Exp Med *213*, 921-928.

Kati, S., Hage, E., Mynarek, M., Ganzenmueller, T., Indenbirken, D., Grundhoff, A., and Schulz, T.F. (2015). Generation of high-titre virus stocks using BrK.219, a B-cell line infected stably with recombinant Kaposi's sarcoma-associated herpesvirus. J Virol Methods *217*, 79-86.

Klein, U., Gloghini, A., Gaidano, G., Chadburn, A., Cesarman, E., Dalla-Favera, R., and Carbone, A. (2003). Gene expression profile analysis of AIDS-related primary effusion lymphoma (PEL) suggests a plasmablastic derivation and identifies PEL-specific transcripts. Blood *101*, 4115-4121.

Krishnan, H.H., Naranatt, P.P., Smith, M.S., Zeng, L., Bloomer, C., and Chandran, B. (2004). Concurrent expression of latent and a limited number of lytic genes with immune modulation and antiapoptotic function by Kaposi's sarcoma-associated herpesvirus early during infection of primary endothelial and fibroblast cells and subsequent decline of lytic gene expression. J Virol *78*, 3601-3620.

Maunders, M.J., Petti, L., and Rowe, M. (1994). Precipitation of the Epstein-Barr virus protein EBNA 2 by an EBNA 3c-specific monoclonal antibody. J Gen Virol *75 (Pt 4)*, 769-778.

Nilsson, K., Bennich, H., Johansson, S.G., and Ponten, J. (1970). Established immunoglobulin producing myeloma (IgE) and lymphoblastoid (IgG) cell lines from an IgE myeloma patient. Clin Exp Immunol *7*, 477-489.

Renne, R., Zhong, W., Herndier, B., McGrath, M., Abbey, N., Kedes, D., and Ganem, D. (1996). Lytic growth of Kaposi's sarcoma-associated herpesvirus (human herpesvirus 8) in culture. Nat Med *2*, 342-346.

Robinson, A.R., Kwek, S.S., and Kenney, S.C. (2012). The B-cell specific transcription factor, Oct-2, promotes Epstein-Barr virus latency by inhibiting the viral immediate-early protein, BZLF1. PLoS Pathog *8*, e1002516.

Schmid, D., Pypaert, M., and Münz, C. (2007). MHC class II antigen loading compartments continuously receive input from autophagosomes. Immunity *26*, 79-92.

Sharma-Walia, N., Krishnan, H.H., Naranatt, P.P., Zeng, L., Smith, M.S., and Chandran, B. (2005). ERK1/2 and MEK1/2 induced by Kaposi's sarcoma-associated herpesvirus (human herpesvirus 8) early during infection of target cells are essential for expression of viral genes and for establishment of infection. J Virol *79*, 10308-10329.

Tedeschi, R., Enbom, M., Bidoli, E., Linde, A., De Paoli, P., and Dillner, J. (2001). Viral load of human herpesvirus 8 in peripheral blood of human immunodeficiency virus-infected patients with Kaposi's sarcoma. J Clin Microbiol *39*, 4269-4273.

Vieira, J., and O'Hearn, P.M. (2004). Use of the red fluorescent protein as a marker of Kaposi's sarcoma-associated herpesvirus lytic gene expression. Virology *325*, 225-240.

White, R.E., Groves, I.J., Turro, E., Yee, J., Kremmer, E., and Allday, M.J. (2010). Extensive co-operation between the Epstein-Barr virus EBNA3 proteins in the manipulation of host gene expression and epigenetic chromatin modification. PLoS One *5*, e13979.

ZIP File

Click here to access/download

ZIP File

supplemental datasets 090517.zip